Desalination and Water Treatment
www.deswater.com

doi: 10.5004/dwt.2020.25840

194 (2020) 110–132
August

Searching for alkali acetates and their mixtures for closed-loop reverse electrodialysis with high cell potential difference and high Gibbs free energy of mixing by thermodynamic modeling

Congyu Zhang, Yubo Xing, Dongping Tao*

Faculty of Metallurgical and Energy Engineering, Kunming University of Science and Technology, Kunming 650093, Yunnan Province, China, emails: dongpingt@aliyun.com (D.P. Tao), sfycong.ok@163.com (C.Y. Zhang), xingyb2015@163.com (Y.B. Xing)

Received 2 September 2019; Accepted 16 March 2020

ABSTRACT

The application of non-conventional salt in closed-loop reverse electrodialysis has attracted much attention. The search for such salt solution is an important first step. In the present work, the activity coefficients, the values of ideal potential difference and Gibbs free energy of mixing of alkali acetates and their mixtures are systematically predicted by electrolyte molecular interaction volume model, and the prediction results are analyzed from the perspective of the variation law of activity coefficients to search the most promising systems. In contrast to the NaCl system and under the same concentration conditions (m = 0.1–3.5 mol kg^{-1}), the ideal potential difference and Gibbs free energy of mixing of the KAc, RbAc and CsAc systems are increased obviously among the pure salt systems, with increases of about 12%–14% and 16%–18%, respectively; while the ideal potential difference and Gibbs free energy of mixing of the KAc + RbAc, KAc + CsAc, and RbAc + CsAc systems are improved obviously among the mixed systems, with increases of about 13% and 17%–18%, respectively. By further comparison, the ideal potential difference and Gibbs free energy of mixing of the mixture are found to be included in the range between the two pure salt cases. Finally, from the thermodynamic modeling point of view, there is no benefit from using the alkali acetate mixtures. The performance of the pure salt2 (a mixture consists of the pure salt1 and the pure salt2) is always superior to that of the mixture, and the pure CsAc system provides almost the maximum values of ideal cell potential difference and Gibbs free energy of mixing.

Keywords: Closed-loop reverse electrodialysis; Alkali acetates; Mixtures; Thermodynamic modeling; Cell potential difference; Gibbs free energy of mixing

1. Introduction

Salinity gradient power is currently attracting more and more attention among the scientific community as renewable energy. In particular, reverse electrodialysis (RED) is emerging as one of the most promising technologies for electricity generation by mixing two solutions of different concentrations [1–4].

However, the operation of open-loop RED with natural water or wastewater streams has some disadvantages, such as the requirement of extensive pretreatment, fouling-control strategies, the lower power density produced, the limited availability of the water resource and the reduction in membranes performances, etc. [2,5]. To overcome the above drawbacks, a closed-loop RED technology has been developed [2,3]. It consists of a RED unit where electricity is produced using the salinity gradient between the two aqueous electrolyte solutions, and a regeneration unit where low-grade heat is used to treat the solutions exiting from the RED unit and restore their initial salinities [3,4]. In contrast to the open-loop scheme, the closed-loop RED avoids the geographical constraint of the limited availability of water streams at

* Corresponding author.

different salinity, increases the power density output and overcomes the limitations associated with possible fouling phenomena, etc. [2,5]. Moreover, the most interesting aspect of closed-loop RED is that it can artificially select an ad-hoc salt solution to enhance the overall performance of the integrated process [6]. In general, a suitable salt for RED applications should have [7]: (i) high solubility in water, (ii) high activity coefficients at high concentrations, and (iii) high equivalent conductivity of the aqueous solution.

A great deal of work has been focused on the application of the conventional single salt solution (i.e. NaCl) in RED stacks [8–11]. And the selection of the salts is also concentrated in the monovalent types, because the presence of multivalent ions in solution has a negative impact on the RED performance, which will likely reduce the magnitude of the power density [12,13].

In recent years, growing attention has been paid to the application of non-conventional salts in RED stacks. Among the aqueous solutions which can be used as working fluid, NH_4HCO_3 aqueous solutions are of great interest due to their potential to utilize very low-grade heat (T = 40°C–100°C). And it can be distilled to CO_2 and NH_3 to form high and low concentration solutions that can be used for salinity gradient energy production [14–17]. However, the solubility limit of this salt (less than 3 M) is a major drawback, limiting the maximum driving force achievable; and the performance of the RED stack with this salt is lower than that with NaCl salt at the same concentrations due to lower activity coefficients [18]. Olkis et al. [19] developed a novel closed-loop RED system with an adsorption desalinator for the restoration of the salts. A variety of the monovalent salts are investigated, the LiCl system gives the best performance because the solubility of this salt is up to 20 molal at room temperature and it has a large activity coefficient at high concentration. Ortega-Delgado et al. [5] compared the performance of the NaCl and KAc systems in the RED-multi effect distillation heat engine; they point out that KAc gives higher thermal efficiency. The better performance of the KAc system is mainly attributed to its higher solubility and higher activity coefficient in comparison with the NaCl system. Tamburini et al. [7] assessed many salt solutions for RED-heat engine applications. The obtained results show that lithium-based salt (e.g. LiBr, LiCl, etc.) and the KAc system provide the highest values of power density in comparison with the NaCl system. This can also be attributed to the fact that those salts have a higher solubility and higher activity coefficients in comparison with the NaCl system. A similar conclusion is also reflected in the work of Giacalone et al. [20]. Recently, Giacalone et al. [6] investigated some non-conventional salt solutions on the operation and performance of closed-loop RED. Results indicate that the LiCl, KAc and CsAc systems appear as the most promising systems, which is also due to their high solubility in water and high activity coefficient at a high concentration so that the Gibbs free energy of mixing is higher. Eventually, the more energy can theoretically be obtained from RED unit.

In contrast, the researches of the multi-component system in the closed-loop RED application are much less. Micari et al. [21] studied some ternary systems on the performance of closed-loop RED. And they found that although the ideal potential differences of the mixed systems are not superior to that of the pure salt cases, some of them have the lower measured stack electrical resistances than both the two values measured for the corresponding pure salts, thus resulting into higher power density values for the mixtures. The NaCl + LiCl, NH_4Cl + LiCl, and NH_4Cl + NaCl systems are identified as the most interesting.

Summarizing, the investigation of RED units fed by non-conventional salt solutions is a very important topic at present. Surprisingly, insufficient work has been done on the performance of pure salts and mixtures in RED units. Hence, to find more efficient solutions and expand the application of some non-conventional salt systems such as alkali acetates in closed-loop RED units, we systematically studied the alkali acetates and their mixtures by electrolyte molecular interaction volume model (eMIVM) [22] from the perspective of thermodynamic modeling (conductivity is not within the scope of this paper) and compared it with NaCl aqueous solution. The ideal potential difference and the Gibbs free energy of mixing are predicted to investigate the performances of the systems studied in this work and to search for the most promising systems.

2. Model descriptions

Herein, we will briefly introduce a predictive model, eMIVM, which has a good statistical thermodynamic basis and the physical meaning of the model parameters is clear. The model consists of two contributions: one from the long-range ion-ion interactions that exist beyond the immediate neighborhood of an ionic species (expressed by the Pitzer–Debye–Hückel equation), and the other from the short-range local interactions that exist at the immediate neighborhood of any species (expressed by the molecular interaction volume model (MIVM) [23]).

2.1. Long-range term

The Pitzer–Debye–Hückel equation for describing the long-range electrostatic interaction of infinite dilute aqueous electrolyte solution to molten salt has empirical effectiveness [24]:

$$\ln\gamma_i^{*,\mathrm{PDH}} = -A_\phi\left(\frac{1{,}000}{M_s}\right)^{1/2}\left[\frac{2z_i^2}{\rho}\ln\left(1+\rho I_x^{1/2}\right)+\frac{z_i^2 I_x^{1/2}-2I_x^{3/2}}{1+\rho I_x^{1/2}}\right]\left(\text{for ion}\right) \tag{1}$$

$$\ln\gamma_s^{\mathrm{PDH}} = \left(\frac{1{,}000}{M_s}\right)^{1/2}\frac{2A_\phi I_x^{3/2}}{1+\rho I_x^{1/2}}\left(\text{for solvent}\right) \tag{2}$$

where the * indicates the unsymmetric convention, i is the component of the solution, x_i is the mole fraction of component i, M_s is the molecular weight of solvent, for water, it's equal to 18.015 g mol^{-1}. T is the absolute temperature. A_ϕ is the Debye–Hückel parameter with a value of 0.3915 at 298.15 K. ρ is the closest approach parameter and a constant value of 14.9 is commonly applied to a wide variety of salts. I_x is the ionic strength of the solution:

$$I_x = \frac{1}{2}\sum_i z_i^2 x_i \tag{3}$$

where z_i is the charge number of ion and z_i is zero for a solvent molecule.

2.2. Short-range term

The molar excess Gibbs energy of the short-range term of the eMIVM is expressed as:

$$\frac{G_m^{\mathrm{ex,MIVM}}}{RT}=-\frac{1}{2}\left[\sum_s Z_s x_s \frac{\sum_j x_j B_{\mathrm{js}}\ln B_{\mathrm{js}}}{\sum_k x_k B_{\mathrm{ks}}}+\sum_c Z_c x_c \sum_{a'}\left(\frac{x_{a'}}{\sum_{a''} x_{a''}}\right)\frac{\sum_j x_j B_{\mathrm{jc},a'c}\ln B_{\mathrm{jc},a'c}}{\sum_k x_k B_{\mathrm{kc},a'c}}+\sum_a Z_a x_a \sum_{c'}\left(\frac{x_{c'}}{\sum_{c''} x_{c''}}\right)\frac{\sum_j x_j B_{\mathrm{ja},c'a}\ln B_{\mathrm{ja},c'a}}{\sum_k x_k B_{\mathrm{ka},c'a}}\right]+\sum_s x_s \ln\left(\frac{V_{\mathrm{ms}}}{\sum_k x_k B_{\mathrm{ks}} V_{\mathrm{mk}}}\right) \tag{4}$$

The right side of Eq. (4) contains the energy term (molecular interaction) and the volume term (microstate number of molecular configuration). The summations over j and k are for all species, S denotes molecular species; c, c' and c'' denote cationic species; a, a' and a'' denote anionic species. Z_i is the coordination number of species and all taken as 10. V_{mi} is the molar volume of species [25]. B denotes the model binary parameters for the energy of interactions. A detailed discussion of the model parameters will be presented in section 2.3. If the solution is electrolyte-free, the eMIVM can be reduced to MIVM.

The activity coefficient of species is given by the partial of the molar excess Gibbs energy function of Eq. (4). For molecular species:

$$\ln\gamma_s^{\mathrm{MIVM}}=-\frac{1}{2}\left[\begin{array}{l} Z_s\dfrac{\sum_j x_j B_{\mathrm{js}}\ln B_{\mathrm{js}}}{\sum_k x_k B_{ks}}+\sum_{s'} Z_{s'}\dfrac{x_{s'}B_{\mathrm{ss}'}}{\sum_k x_k B_{\mathrm{ks}'}}\left(\ln B_{\mathrm{ss}'}-\dfrac{\sum_k x_k B_{\mathrm{ks}'}\ln B_{\mathrm{ks}'}}{\sum_k x_k B_{\mathrm{ks}'}}\right)+\sum_c Z_c\sum_{a'}\left(\dfrac{x_{a'}}{\sum_{a''} x_{a''}}\right)\dfrac{x_c B_{\mathrm{sc},a'c}}{\sum_k x_k B_{\mathrm{kc},a'c}}\left(\ln B_{\mathrm{sc},a'c}-\dfrac{\sum_k x_k B_{\mathrm{kc},a'c}\ln B_{\mathrm{kc},a'c}}{\sum_k x_k B_{\mathrm{kc},a'c}}\right)+ \\ \sum_a Z_a\sum_{c'}\left(\dfrac{x_{c'}}{\sum_{c''} x_{c''}}\right)\dfrac{x_a B_{\mathrm{sa},c'a}}{\sum_k x_k B_{\mathrm{ka},c'a}}\left(\ln B_{\mathrm{sa},c'a}-\dfrac{\sum_k x_k B_{\mathrm{ka},c'a}\ln B_{\mathrm{ka},c'a}}{\sum_k x_k B_{\mathrm{ka},c'a}}\right) \end{array}\right] +\ln\left(\frac{V_{\mathrm{ms}}}{\sum_k x_k B_{\mathrm{ks}} V_{\mathrm{mk}}}\right)+\sum_{s'} x_{s'}\left(1-\frac{B_{\mathrm{ss}'}V_{\mathrm{ms}}}{\sum_k x_k B_{\mathrm{ks}'}V_{\mathrm{mk}}}\right) \tag{5}$$

For cations:

$$\ln\gamma_c^{\mathrm{MIVM}}=-\frac{1}{2}\left[\begin{array}{l} Z_c\sum_{a'}\left(\dfrac{x_{a'}}{\sum_{a''} x_{a''}}\right)\dfrac{\sum_k x_k B_{\mathrm{kc},a'c}\ln B_{\mathrm{kc},a'c}}{\sum_k x_k B_{\mathrm{kc},a'c}}+\sum_s Z_s\dfrac{x_s B_{\mathrm{cs}}}{\sum_k x_k B_{\mathrm{ks}}}\left(\ln B_{\mathrm{cs}}-\dfrac{\sum_k x_k B_{\mathrm{ks}}\ln B_{\mathrm{ks}}}{\sum_k x_k B_{\mathrm{ks}}}\right)+\sum_a Z_a\sum_{c'}\left(\dfrac{x_{c'}}{\sum_{c''} x_{c''}}\right)\dfrac{x_a B_{\mathrm{ca},c'a}}{\sum_k x_k B_{\mathrm{ka},c'a}} \\ \left(\ln B_{\mathrm{ca},c'a}-\dfrac{\sum_k x_k B_{\mathrm{ka},c'a}\ln B_{\mathrm{ka},c'a}}{\sum_k x_k B_{\mathrm{ka},c'a}}\right) \end{array}\right] +\sum_s x_s\left(1-\frac{B_{\mathrm{cs}}V_{\mathrm{mc}}}{\sum_k x_k B_{\mathrm{ks}}V_{\mathrm{mk}}}\right) \tag{6}$$

For anions:

$$\ln\gamma_a^{\mathrm{MIVM}}=-\frac{1}{2}\left[\begin{array}{l} Z_a\sum_{c'}\left(\dfrac{x_{c'}}{\sum_{c''} x_{c''}}\right)\dfrac{\sum_k x_k B_{\mathrm{ka},c'a}\ln B_{\mathrm{ka},c'a}}{\sum_k x_k B_{\mathrm{ka},c'a}}+\sum_s Z_s\dfrac{x_s B_{\mathrm{as}}}{\sum_k x_k B_{\mathrm{ks}}}\left(\ln B_{\mathrm{as}}-\dfrac{\sum_k x_k B_{\mathrm{ks}}\ln B_{\mathrm{ks}}}{\sum_k x_k B_{\mathrm{ks}}}\right)+\sum_c Z_c\sum_{a'}\left(\dfrac{x_{a'}}{\sum_{a''} x_{a''}}\right)\dfrac{x_c B_{\mathrm{ac},a'c}}{\sum_k x_k B_{\mathrm{kc},a'c}} \\ \left(\ln B_{\mathrm{ac},a'c}-\dfrac{\sum_k x_k B_{\mathrm{kc},a'c}\ln B_{\mathrm{kc},a'c}}{\sum_k x_k B_{\mathrm{kc},a'c}}\right) \end{array}\right] +\sum_s x_s\left(1-\frac{B_{\mathrm{as}}V_{\mathrm{ma}}}{\sum_k x_k B_{\mathrm{ks}}V_{\mathrm{mk}}}\right) \tag{7}$$

To obtain the unsymmetric short-range activity coefficients of ions, the following equations should be used:

$$\ln\gamma_c^{*,\mathrm{MIVM}}=\ln\gamma_c^{\mathrm{MIVM}}-\ln\gamma_c^{\mathrm{MIVM},\infty} \tag{8}$$

$$\ln\gamma_a^{*,\mathrm{MIVM}}=\ln\gamma_a^{\mathrm{MIVM}}-\ln\gamma_a^{\mathrm{MIVM},\infty} \tag{9}$$

The corresponding activity coefficients at the infinite dilution limit of the aqueous solution can be calculated as:

$$\ln\gamma_c^{\mathrm{MIVM},\infty} = -\frac{1}{2}\left(Z_s B_{\mathrm{cs}}\ln B_{\mathrm{cs}} + Z_c\sum_{a'}\frac{x_{a'}\ln B_{\mathrm{sc},a'c}}{\sum_{a''}x_{a''}}\right) + \left(1-\frac{B_{\mathrm{cs}}V_{\mathrm{sc}}}{V_{\mathrm{ms}}}\right) \quad (10)$$

$$\ln\gamma_a^{\mathrm{MIVM},\infty} = -\frac{1}{2}\left(Z_s B_{\mathrm{as}}\ln B_{\mathrm{as}} + Z_a\sum_{c'}\frac{x_{c'}\ln B_{\mathrm{sa},c'a}}{\sum_{c''}x_{c''}}\right) + \left(1-\frac{B_{\mathrm{as}}V_{\mathrm{ma}}}{V_{\mathrm{ms}}}\right) \quad (11)$$

where $\gamma_c^{\mathrm{MIVM},\infty}$ and $\gamma_a^{\mathrm{MIVM},\infty}$ are the activity coefficients at infinite dilution aqueous solution.

Therefore, the unsymmetric activity coefficient expression of the eMIVM is expressed as:

$$\ln\gamma_I^{*,\mathrm{eMIVM}} = \ln\gamma_i^{*,\mathrm{PDH}} + \ln\gamma_i^{*,\mathrm{MIVM}} \quad (12)$$

The mean activity coefficient of electrolyte is defined as:

$$\ln\gamma_\pm^* = \frac{1}{\nu}\left(\nu_c\ln\gamma_c^* + \nu_a\ln\gamma_a^*\right) \quad (13)$$

where ν_c and ν_a are the numbers of cations and anions in the neutral salt. Also $\nu = \nu_a + \nu_c$.

As the experimental data available in the literature are normalized in molality scale and the activity coefficients calculated from the eMIVM are in mole fraction scale, so the following conversion should be used:

$$\ln\gamma_{\pm m}^* = \ln\gamma_\pm^* - \ln\left[1+0.001M_s\sum_i m_i\right] \quad (14)$$

where $\gamma_\pm^*$ is the mole fraction scale mean ionic activity coefficient; $\gamma_{\pm m}^*$ is the molality scale mean ionic activity coefficient; m_i is the molality of ion i, mol kg^{-1}. The osmotic coefficient is defined as:

$$\phi = -\left(\frac{1{,}000}{M_s\sum_i m_i}\right)\ln\left(x_s\gamma_s\right) \quad (15)$$

2.3. Model parameters

For a binary system, $B_{\mathrm{ca},s}$ and $B_{\mathrm{s,ca}}$ are the only two adjustable electrolyte-specific parameters, and defined as:

$$B_{\mathrm{as}} = B_{\mathrm{cs}} = B_{\mathrm{ca},s} \quad (16)$$

$$B_{\mathrm{sa,ca}} = B_{\mathrm{sc,ac}} = B_{\mathrm{s,ca}} \quad (17)$$

B parameters are expressed as:

$$B_{\mathrm{ji}} = \exp\left(-\frac{\varepsilon_{ji}-\varepsilon_{ii}}{kT}\right) \quad (18)$$

$$B_{ji,li} = \frac{B_{ji}}{B_{li}} = \exp\left(-\frac{\varepsilon_{ji}-\varepsilon_{li}}{kT}\right) \quad (19)$$

ε_{ii} is the $i-i$ pair-potential energy, others are similar.

For a multi-component system, B_{cs} and B_{as} can be generalized to:

$$B_{\mathrm{cs}} = \frac{\sum_a z_a x_a B_{\mathrm{ca},s}}{\sum_{a'} z_{a'}x_{a'}} \quad (20)$$

$$B_{\mathrm{as}} = \frac{\sum_c z_c x_c B_{\mathrm{ca},s}}{\sum_{c'} z_{c'}x_{c'}} \quad (21)$$

$B_{\mathrm{ca},s}$ in Eqs. (20) and (21) is the binary parameter.

The variables $B_{\mathrm{sa,ca}}$ and $B_{\mathrm{sc,ac}}$ can be calculated from the B_{is} (Eqs. (20) and (21)):

$$\begin{aligned} B_{\mathrm{sa,ca}} &= \exp\left(-\frac{\varepsilon_{\mathrm{sa}}-\varepsilon_{\mathrm{ca}}}{kT}\right) = \exp\left(-\frac{\varepsilon_{\mathrm{sa}}-\varepsilon_{\mathrm{ss}}}{kT}-\frac{\varepsilon_{\mathrm{ss}}-\varepsilon_{\mathrm{ca}}}{kT}\right) \\ &= \frac{\exp\left(-\frac{\varepsilon_{\mathrm{sa}}-\varepsilon_{\mathrm{ss}}}{kT}\right)\exp\left(-\frac{\varepsilon_{\mathrm{sa}}-\varepsilon_{\mathrm{ca}}}{kT}\right)}{\exp\left(-\frac{\varepsilon_{\mathrm{sa}}-\varepsilon_{\mathrm{ss}}}{kT}\right)} \\ &= \frac{B_{\mathrm{as}}B_{s,\mathrm{ca}}}{B_{\mathrm{ca},s}} \end{aligned} \quad (22)$$

and

$$B_{\mathrm{sc,ac}} = \frac{B_{\mathrm{cs}}B_{s,\mathrm{ca}}}{B_{\mathrm{ca},s}} \quad (23)$$

Furthermore, the salt–salt binary interaction parameters are also required in the eMIVM, and these parameters are handled as follows:

$$B_{\mathrm{ca},c'a} = \exp\left(-\frac{\varepsilon_{\mathrm{ca}}-\varepsilon_{c'a}}{kT}\right) = \frac{1}{\exp\left(-\frac{\varepsilon_{c'a}-\varepsilon_{\mathrm{ca}}}{kT}\right)} = \frac{1}{B_{c'a,\mathrm{ca}}} \quad (24)$$

and

$$B_{\mathrm{ca,ca'}} = \frac{1}{B_{\mathrm{ca',ca}}} \quad (25)$$

Determination of the salt–salt binary interaction parameter is obtained by fitting of solubility data or activity and osmotic coefficient data in the ternary system. It can be seen that $B_{\mathrm{ca},s}$, $B_{s,\mathrm{ca}}$, $B_{\mathrm{ss'}}$, $B_{s's}$, $B_{\mathrm{ca},c'a}$, $B_{c'a,\mathrm{ca}}$, $B_{\mathrm{ca,ca'}}$, and $B_{\mathrm{ca',ca}}$ are the adjustable binary parameters for the multi-component system. Specifically, for a ternary system with only one solvent component and a common anion, the $B_{\mathrm{ss'}}$, $B_{s's}$, $B_{\mathrm{ca',ca}}$, and $B_{\mathrm{ca,ca'}}$ are equal to unity.

The molar volumes of species are required in the eMIVM. For the sake of simplicity, the ions are treated as spherical; so the molar volumes of ions can be calculated by the following formula [25]:

$$V_{\mathrm{mi}} = \left(\frac{4\pi N_A}{3}\right)r_i^3 = 2522.5r_i^3 \quad (26)$$

where N_A is the Avogadro constant, r_i (nm) is the ion radius in aqueous solution. The molar volume of pure water (V_{ms}) is 18.07 cm^3 mol^{-1} at 298.15 K. The values of the ionic radii are taken from reference [26], and the corresponding values and the ionic molar volumes are listed in Table 1.

3. Binary systems

3.1. Model parameter regression

The binary parameters $B_{ca,s}$ and $B_{s,ca}$ of eMIVM are evaluated from the experimental osmotic coefficient data compiled by Robinson and Stokes [27] at 298.15 K with the least square method. The model parameters and the correlation results are shown in Table 2.

Table 1
Ionic radii and the molar volumes of ions [26]

Ion	r_i (nm)	V_{mi} (cm^3 mol^{-1})
Li^+	0.069	0.83
Na^+	0.102	2.68
K^+	0.138	6.63
Rb^+	0.149	8.34
Cs^+	0.170	12.39
Cl^-	0.181	14.96
Br^-	0.196	18.99
Ac^-	0.232	31.50

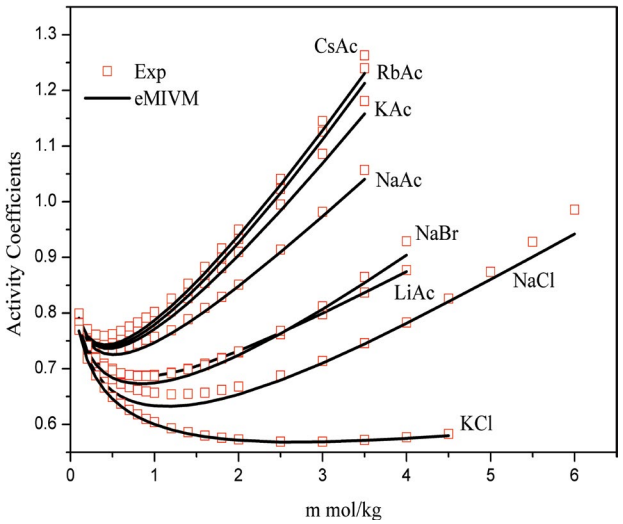

Fig. 2. Prediction of activity coefficients using eMIVM for various electrolyte systems at 298.15 K [27].

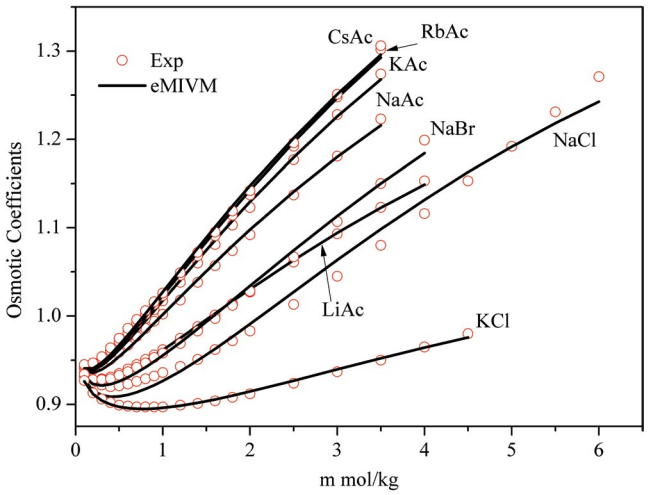

Fig. 1. Fitting results of osmotic coefficients of eMIVM for various electrolyte systems at 298.15 K [27].

Table 2
Binary adjustable parameters and the calculation deviations of the eMIVM for various electrolytes at 298.15 K [27]

Electrolyte	$B_{ca,s}$	$B_{s,ca}$	Data fit	SD[a]-OS	ARD%[b]-OS	Data predict	SD-AC	ARD%-AC	m-mol kg^{-1}
NaCl	2.4915	0.1652	OS	0.0122	1.03	AC	0.0196	2.37	0.1–6.0
NaBr	2.4696	0.1714	OS	0.0061	0.53	AC	0.0119	1.50	0.1–4.0
KCl	2.2437	0.2019	OS	0.0020	0.20	AC	0.0029	0.42	0.1–4.5
LiAc	2.2970	0.1974	OS	0.0023	0.20	AC	0.0035	0.39	0.1–4.0
NaAc	2.3339	0.1966	OS	0.0042	0.38	AC	0.0088	1.01	0.1–3.5
KAc	2.3649	0.1896	OS	0.0044	0.39	AC	0.0125	1.41	0.1–3.5
RbAc	2.3874	0.1845	OS	0.0051	0.44	AC	0.0130	1.42	0.1–3.5
CsAc	2.3496	0.1887	OS	0.0057	0.49	AC	0.0160	1.76	0.1–3.5
Average (8)				0.0053	0.46		0.0110	1.29	

OS refers to osmotic coefficient
AC refers to activity coefficient

[a] $$\mathrm{SD}=\sqrt{\frac{1}{\mathrm{NP}}\sum\left(\phi^{\mathrm{exp}}-\phi^{\mathrm{cal}}\right)^2}\ \text{or}\ \mathrm{SD}=\sqrt{\frac{1}{\mathrm{NP}}\sum\left(\gamma_{\pm}^{\mathrm{exp}}-\gamma_{\pm}^{\mathrm{cal}}\right)^2}$$

[b] $$\mathrm{ARD}\%=\frac{1}{\mathrm{NP}}\sum\left|\frac{\phi^{\mathrm{exp}}-\phi^{\mathrm{cal}}}{\phi^{\mathrm{exp}}}\right|\times 100\%\ \text{or}\ \mathrm{ARD}\%=\frac{1}{\mathrm{NP}}\sum\left|\frac{\gamma_{\pm}^{\mathrm{exp}}-\gamma_{\pm}^{\mathrm{cal}}}{\gamma_{\pm}^{\mathrm{exp}}}\right|\times 100\%$$

It can be seen from Table 2 that the fitting concentrations of 8 binary systems are limited below 6 mol kg^{-1}. Overall, eMIVM has a good fitting effect on the systems studied in this work and the results are in good agreement with the experimental data, with the mean standard deviation (SD) and the average relative deviation (ARD%) being 0.0053 and 0.46%, respectively. The fitting accuracy of the model for the alkali acetate systems decreases gradually from LiAc to CsAc. In contrast to other systems, this model has the worst correlation effect for the NaCl system, with the SD and ARD% being 0.0122 and 1.03%, respectively. Fig. 1 shows the model fitting results.

3.2. Activity coefficients

The model binary parameters given in Table 2 are used for the prediction of activity coefficient data for the same electrolytes, and the results are still shown in the same table. In contrast to the fitting results, the average prediction accuracy of the model is reduced by about two times, and the SD and ARD% are 0.0110% and 1.29%, respectively. As can be seen from Fig. 2, the change rule of the activity coefficient of salts satisfies KCl < NaCl < LiAc < NaBr < NaAc < KAc < RbAc < CsAc; more precisely, at m = 0.1 mol kg^{-1}, the activity coefficient values of alkali acetates (from LiAc to CsAc) are about 0.77%–2.70% higher than that of the NaCl salt, while at m = 3.5 mol kg^{-1}, the activity coefficient values of alkali acetates are about 12%–69% higher than that of the NaCl salt.

3.3. Ideal cell potential difference

In this work, we use the NaCl system as the reference case and assume that the feed solution in the concentrate compartment and the dilute compartment contains 1 kg of water and m-high (mol kg^{-1}) of salt as well as 1 kg of water and m-low (mol kg^{-1}) of salt at 298.15 K (typical working temperature of RED units), respectively. The salt concentration is limited as follows: m-high = 3.5 mol kg^{-1} and m-low = 0.1 mol kg^{-1}. The ideal cell potential difference (i.e. ideal membranes, permselectivity α_p = 1) is related to the open-circuit voltage (OCV) of RED units. The latter is important data for RED units that can be measured experimentally [21]. Once activity coefficients of salts have been calculated, then the cell potential difference-$\Delta\phi_{\text{cell-pure}}$ of pure salt can be calculated through the Nernst equation as follows [21]:

$$\Delta\phi_{\text{cell}-\text{pure}} = \frac{RT}{F}\ln\left(\frac{a_c^{\text{high}}a_a^{\text{high}}}{a_c^{\text{low}}a_a^{\text{low}}}\right) = \frac{2RT}{F}\ln\left(\frac{a_{\text{salt}}^{\text{high}}}{a_{\text{salt}}^{\text{low}}}\right) = \frac{2RT}{F}\ln\left(\frac{m_{\text{salt}}^{\text{high}}\gamma_{\pm\text{salt}}^{*\text{high}}}{m_{\text{salt}}^{\text{low}}\gamma_{\pm\text{salt}}^{*\text{low}}}\right) \tag{27}$$

where F is the Faraday constant (96,485 J C^{-1}) and a is the activity of salt. The values of $\Delta\phi_{\text{cell-pure}}$ are listed in Table 3.

As discussed in section 3.2, the difference of activity coefficient values of each salt at 0.1 mol kg^{-1} is very small, and the difference of the activity coefficient values increases with the increase of the concentration. Therefore, it can be seen from Eq. (27) that the higher the activity coefficient values of salts at high concentration, the greater the $\Delta\phi_{\text{cell-pure}}$ values. The changes in the $\Delta\phi_{\text{cell-pure}}$ values shown in Table 3 confirm the above viewpoints, and their values are consistent with the changes in activity coefficient values of salts. In contrast to the NaCl system, the $\Delta\phi_{\text{cell-pure}}$ values increase in different degrees, namely, NaCl < LiAc < NaAc < KAc < RbAc < CsAc. Among them, the KAc, RbAc, and CsAc systems exhibit relatively significant performance improvements, with an increase of about 12%–14%. It is anticipated that these three salts will have higher OCV in closed-loop RED units.

3.4. Gibbs free energy of mixing

The Gibbs free energy of mixing ($\Delta_{\text{mix}}G$) represents the theoretical maximum energy that can be obtained from the salinity gradient, regardless of dissipative phenomena. As a matter of fact, the actual amount of useful energy will always be less than $\Delta_{\text{mix}}G$. Nonetheless, the Gibbs free energy of mixing is useful for assessing the magnitude of potential power generation with salinity gradients [28]. The Gibbs free energy (G_{solution}) of a pure salt solution can be defined as [29]:

$$\begin{aligned} G_{\text{solution}} &= n_{\text{salt}}\mu_{\text{salt}} + n_w\mu_w \\ &= n_{\text{salt}}\mu_{\text{salt}}^{\Theta} + \nu n_{\text{salt}}RT\ln\left(m_{\text{salt}}\gamma_{\pm\text{salt}}\right) + n_w\left(\mu_w^{O} - RT\frac{\nu m_{\text{salt}}M_s}{1{,}000}\phi\right) \end{aligned} \tag{28}$$

where n_{salt} and n_w are the moles of salt and water, respectively. ν = 2 (1–1 type salt), $\mu_{\text{salt}}^{\Theta}$ is the chemical potential of salt in the standard state (i.e. ideal 1 molal solution at 298.15 K and 1 atm), μ_w^{O} is the solvent chemical potential

Table 3
Results of the ideal cell potential difference and the Gibbs free energy of mixing for pure salts at 298.15 K

Electrolyte	m-low	m-high	$\Delta\phi_{\text{cell}}$ (V)	ARD%[a]	$-\Delta_{\text{mix}}G$ (KJ)	ARD%[a]
NaCl	0.1	3.5	0.1809		10.5758	
LiAc	0.1	3.5	0.1863	2.99	10.9477	3.52
NaAc	0.1	3.5	0.197	8.90	11.8021	11.60
KAc	0.1	3.5	0.2024	11.89	12.2494	15.83
RbAc	0.1	3.5	0.2047	13.16	12.4493	17.72
CsAc	0.1	3.5	0.2054	13.54	12.4982	18.18

[a]ARD% – compared to NaCl

in the standard state. The Gibbs free energy of mixing is evaluated as the difference between the Gibbs free energy of the solution resulting from the mixing (G_{mix}) and the Gibbs free energy of the two initial feed solutions (i.e., G_{low} and G_{high}) [6]:

$$\Delta_{mix}G = G_{mix} - G_{low} - G_{high} \tag{29}$$

In more detail, Eq. (29) can be derived as:

$$\Delta_{mix}G = vRTn_{mix}\left[\ln\left(m_{mix}\gamma_{\pm mix}\right) - \phi_{mix}\right] - vRTn_{low}\left[\ln\left(m_{low}\gamma_{\pm low}\right) - \phi_{low}\right] - vRTn_{high}\left[\ln\left(m_{high}\gamma_{\pm high}\right) - \phi_{high}\right] \tag{30}$$

As one can see from Table 3, the $\Delta_{mix}G$ value of each salt is higher than that of the NaCl system to some extent, and the $\Delta_{mix}G$ value satisfies NaCl < LiAc < NaAc < KAc < RbAc < CsAc. In contrast to the NaCl system, the smallest improvement is the LiAc system, with an increase of about 3.5%, while the KAc, RbAc and CsAc systems exhibit obvious performance improvements, with an increase of about 16%–18%, which is consistent with the results of the study on the NaCl, KAc and CsAc systems using Pitzer's equation by Giacalone et al. [6].

It can be considered that the $\Delta\phi_{cell\text{-}pure}$ and $\Delta_{mix}G$ values of alkali acetates are higher than those of the NaCl system under the same concentration conditions, and the KAc, RbAc, and CsAc systems show relatively obvious performance improvements.

4. Ternary systems

4.1. Model validation

Five single alkali acetate systems can form ten ternary mixtures, namely, the LiAc + NaAc, LiAc + KAc, LiAc + RbAc, LiAc + CsAc, NaAc + KAc, NaAc + RbAc, NaAc + CsAc, KAc + RbAc, KAc + CsAc and RbAc + CsAc systems. To the best of our knowledge, only the experimental data of the LiAc + NaAc [30] and NaAc + KAc [31] systems are available in the literature. Therefore, we also looked for some mixtures containing alkali acetates as verification systems because these systems may have similar properties to the mixtures predicted in this work. However, these verification systems basically composed of the NaAc or KAc system, and the experimental data for the ternary systems containing the RbAc or CsAc system are not reported. Table 4 shows the comparison of the prediction results of eMIVM (using model binary parameters as shown in Table 2) with the experimental data. Fig. 3 presents the model prediction examples of the LiAc + NaAc and the NaAc + KAc systems.

In general, the prediction effects of eMIVM are satisfactory and the results are in good agreement with the experimental data, and the average SD and ARD% are 0.0110 and 1.15%, respectively. Moreover, according to our previous work, eMIVM is able to predict well for a variety of ternary systems containing K, Rb, and Cs (please see reference [22] and Table S11). Hence, we believe that eMIVM can also provide convincing predictions for the alkali acetate mixtures studied in this work. Here, we consider that each mixture consists of the same molal amount of the two salts, and the predicted concentration range is I = 0.1–3.5 mol kg^{-1}. The prediction results are listed in the supporting information section S1.

4.2. Activity coefficients

The prediction results of eMIVM reveal several characteristics of activity coefficients of alkali acetate mixtures: (i) if the activity coefficients of the two pure salts are

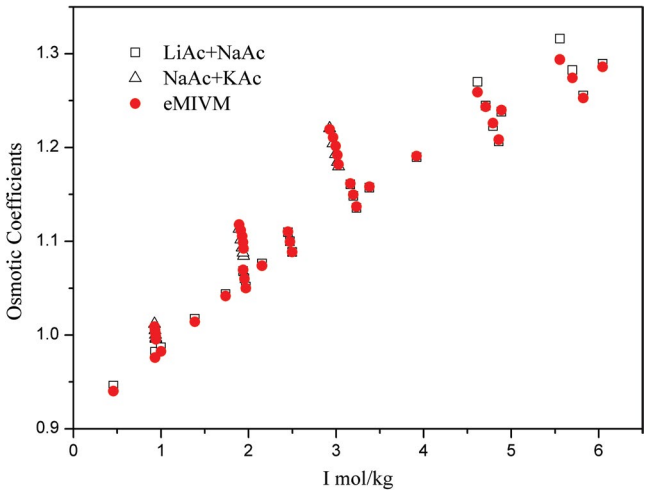

Fig. 3. Prediction of osmotic coefficients of the LiAc + NaAc and the NaAc + KAc systems using eMIVM at 298.15 K [30,31].

Table 4
Prediction results of eMIVM for various mixtures containing alkali acetate salts at 298.15 K

Mixtures	SD-eMIVM	ARD%-eMIVM	Data	I-mol kg^{-1}	Reference
LiAc + NaAc	0.0057	0.30	OS	0.46–6.05	Robinson et al. [30]
NaAc + KAc	0.0065	0.47	OS	0.94–2.93	Jones and Prue [31]
NaCl + NaAc	0.0062	0.52	OS	1.89–3.12	Jones and Prue [31]
NaCl(*A*) + NaAc(*B*)	0.0284	2.86	AC-*A*	1.0–5.0	Lanier [32]
NaCl(*A*) + NaAc(*B*)	0.0186	2.59	AC-*A*	1.0–3.0	Manohar and Ananthaswamy [33]
NaBr(*A*) + NaAc(*B*)	0.0091	1.08	AC-*A*	0.1–3.5	Hernández-Luis et al. [34]
KCl + KAc	0.0028	0.22	OS	0.94–3.17	Jones and Prue [31]
Overall (7)	0.0110	1.15			

$\gamma_{\pm salt1,pure} < \gamma_{\pm salt2,pure}$, then the mixture can still be $\gamma_{\pm salt1,mix} < \gamma_{\pm salt2,mix}$, and the increase or decrease of $\gamma_{\pm salt1,mix}$ or $\gamma_{\pm salt2,mix}$ relative to the pure salt depends on the combination of different salts. From the results of the model predictions, with the exception of the KAc + CsAc and RbAc + CsAc systems, other mixtures can meet the requirements of $\gamma_{\pm salt1,mix} > \gamma_{\pm salt1,pure}$ and $\gamma_{\pm salt2,mix} < \gamma_{\pm salt2,pure}$, Fig. 4 shows an example of the LiAc + RbAc system; (ii) if the mixture contains the same salt1, then the activity coefficient of the salt2 in the mixture follows the change rule of the activity coefficient of the corresponding pure salt. For example, if the salt1 is LiAc, then the activity coefficient of the salt2 follows $\gamma_{\pm NaAc,mix} < \gamma_{\pm KAc,mix} < \gamma_{\pm RbAc,mix} < \gamma_{\pm CsAc,mix}$ as shown in Fig. 5 and; (iii) if the mixture composed of pure salt with a relatively large activity coefficient, then the activity coefficient of each salt in that mixture is also relatively large (compared to other mixtures). For example, the activity coefficients of the KAc + CsAc system are higher than those of the NaAc + RbAc system, namely, $\gamma_{\pm KAc,mix} > \gamma_{\pm NaAc,mix}$ and $\gamma_{\pm CsAc,mix} > \gamma_{\pm RbAc,mix}$ as shown in Fig. 6.

4.3. Ideal cell potential difference

Again, we assume that the feed solutions in the RED compartments contain 1 kg of water and the same molal amount of salt1 and salt2 (m_{tot}-high of concentrate and m_{tot}-low of dilute, $m_{tot} = m_{salt1} + m_{salt2}$) at 298.15 K, and the predicted concentration of the model is limited below 3.5 mol kg^{-1}. In addition, the total concentration of the mixed system is consistent with that of the pure salt system. For ternary systems and ideal membranes (i.e. permselectivity $\alpha_p = 1$), the multi-component Nernst equation can be expressed as follows [21]:

$$\Delta\phi_{cell\text{-}mix} = \frac{RT}{2F}\ln\left(\frac{a_{c1}^{high}a_{c2}^{high}a_{a1}^{high}a_{a2}^{high}}{a_{c1}^{low}a_{c2}^{low}a_{a1}^{low}a_{a2}^{low}}\right) = \frac{RT}{F}\left(\frac{a_{salt1}^{high}a_{salt2}^{high}}{a_{salt1}^{low}a_{salt2}^{low}}\right) = \frac{RT}{F}\left(\frac{m_{salt1}^{high}\gamma_{\pm salt1}^{*high}m_{salt2}^{high}\gamma_{\pm salt2}^{*high}}{m_{salt1}^{low}\gamma_{\pm salt1}^{*low}m_{salt2}^{low}\gamma_{\pm salt2}^{*low}}\right) \quad (31)$$

where number 2 at the denominator is related to the number of salts present in the solution.

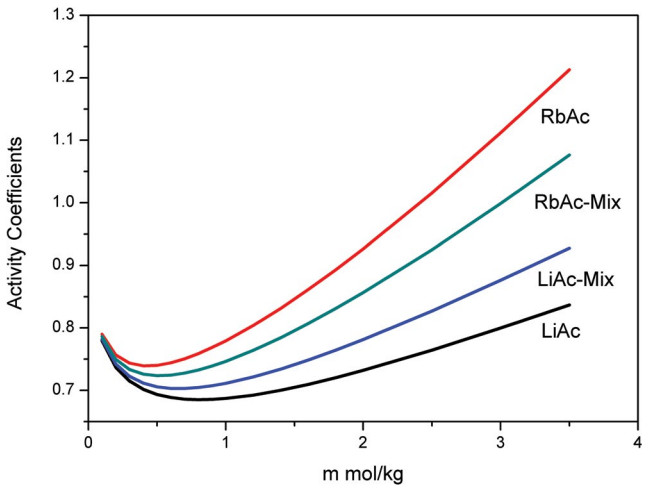

Fig. 4. Activity coefficients of LiAc and RbAc in water vs. solution molality as pure salts and in the LiAc + RbAc mixture.

The $\Delta\phi_{cell\text{-}mix}$ values of the mixed systems can be calculated by the activity coefficients given in the supporting information section S1. Table 5 summarizes the $\Delta\phi_{cell\text{-}mix}$ values.

In the mixed systems, the difference of activity coefficient values of each salt at low concentration (i.e. m = 0.1 mol kg^{-1}) is very small (supporting information section S1). Therefore, according to Eq. (31), the value of $\Delta\phi_{cell\text{-}mix}$ depends on the activity coefficient at high concentration. According to the analysis in section 4.2, with LiAc as salt1, the activity coefficient value of another salt2 in the mixture increases gradually from NaAc to CsAc. Hence, the $\Delta\phi_{cell\text{-}mix}$ values of the mixtures with LiAc as salt1 satisfy LiAc + NaAc < LiAc + KAc < LiAc + RbAc < LiAc + CsAc. Similarly, the mixture using the NaAc or KAc or RbAc system as salt1 also satisfies the same rule. Moreover, the mixture composed of pure salt (as salt1) with relatively large activity coefficient (compared to other pure salts set as salt1), the activity coefficient of salt2 in

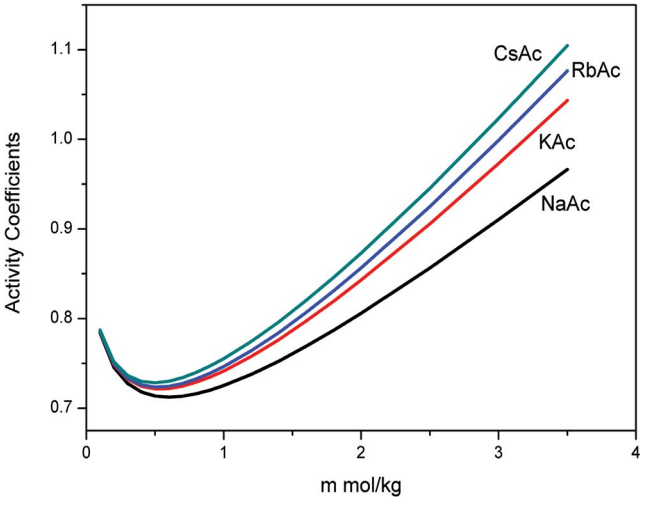

Fig. 5. Activity coefficients of NaAc, KAc, RbAc, and CsAc in the mixtures containing LiAc.

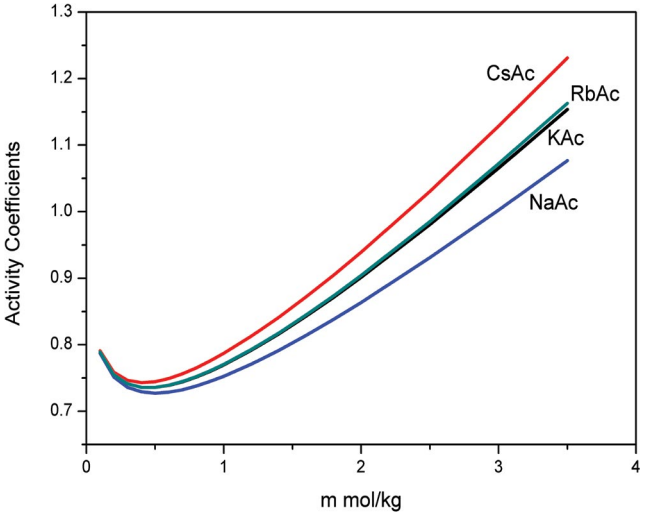

Fig. 6. Comparison of activity coefficients of the NaAc + RbAc and KAc + CsAc systems.

Table 5
Results of the ideal cell potential difference and the Gibbs free energy of mixing for alkali acetate mixtures at 298.15 K

Salt1 + Salt2	m_{tot}-low	m_{tot}-high	$\Delta\phi_{cell\text{-}mix}$ (V)	ARD%[a]	$-\Delta_{mix}G$ (KJ)	ARD%[a]
LiAc + NaAc	0.1	3.5	0.1916	5.92	11.3743	7.55
LiAc + KAc	0.1	3.5	0.1941	7.30	11.5810	9.51
LiAc + RbAc	0.1	3.5	0.1951	7.85	11.6700	10.35
LiAc + CsAc	0.1	3.5	0.1954	8.02	11.6839	10.48
NaAc + KAc	0.1	3.5	0.1996	10.34	12.0225	13.68
NaAc + RbAc	0.1	3.5	0.2007	10.95	12.1148	14.55
NaAc + CsAc	0.1	3.5	0.2009	11.06	12.1308	14.70
KAc + RbAc	0.1	3.5	0.2035	12.49	12.3494	16.77
KAc + CsAc	0.1	3.5	0.2038	12.66	12.3696	16.96
RbAc + CsAc	0.1	3.5	0.2050	13.32	12.4691	17.90

[a]ARD% – compared to NaCl

the mixture is also relatively large, and hence, the $\Delta\phi_{cell\text{-}mix}$ values of the mixtures containing RbAc (as salt1) are the largest, while the $\Delta\phi_{cell\text{-}mix}$ values of the mixtures containing LiAc (as salt1) are the smallest. From the above analysis, the change rule of ideal cell potential difference of each mixture in Table 5 can be obtained. Since the KAc + RbAc, KAc + CsAc and RbAc + CsAc systems have relatively large activity coefficient values, thus they can give a larger $\Delta\phi_{cell\text{-}mix}$ value, which is about 13% higher than that of the NaCl system. It can be considered that these three mixtures will have higher OCV in closed-loop RED units.

4.4. Gibbs free energy of mixing

Similar to section 3.4, the Gibbs free energy of a ternary system containing the two 1–1 type salts can be derived as follows [29]:

$$\begin{aligned} G_{solution} &= n_{salt1}\mu_{salt1} + n_{salt2}\mu_{salt2} + n_w\mu_w \\ &= n_{salt1}\left[\mu^{\Theta}_{salt1} + \nu_1 RT\ln\left(m_{salt1}\gamma_{\pm salt1}\right)\right] \\ &+ n_{salt2}\left[\mu^{\Theta}_{salt2} + \nu_2 RT\ln\left(m_{salt2}\gamma_{\pm salt2}\right)\right] \\ &+ n_w\left[\mu^{O}_{w} - RT\frac{\left(\nu_1 m_{salt1} + \nu_2 m_{salt2}\right)M_w}{1{,}000}\phi\right] \end{aligned} \tag{32}$$

By using Eq. (32), the Gibbs free energy of mixing $\Delta_{mix}G$ of a ternary system can be obtained as follows:

$$\begin{aligned} \Delta_{mix}G &= G_{mix} - G_{low} - G_{high} \\ &= \nu_1 RT\left(n_{salt1}\right)_{mix}\left\{\ln\left[\left(m_{salt1}\right)_{mix}\left(\gamma_{\pm salt1}\right)_{mix}\right] - \phi_{mix}\right\} \\ &- \nu_1 RT\left(n_{salt1}\right)_{low}\left\{\ln\left[\left(m_{salt1}\right)_{low}\left(\gamma_{\pm salt1}\right)_{low}\right] - \phi_{low}\right\} \\ &- \nu_1 RT\left(n_{salt1}\right)_{high}\left\{\ln\left[\left(m_{salt1}\right)_{high}\left(\gamma_{\pm salt1}\right)_{high}\right] - \phi_{high}\right\} \\ &+ \nu_2 RT\left(n_{salt2}\right)_{mix}\left\{\ln\left[\left(m_{salt2}\right)_{mix}\left(\gamma_{\pm salt2}\right)_{mix}\right] - \phi_{mix}\right\} \\ &- \nu_2 RT\left(n_{salt2}\right)_{low}\left\{\ln\left[\left(m_{salt2}\right)_{low}\left(\gamma_{\pm salt2}\right)_{low}\right] - \phi_{low}\right\} \\ &- \nu_2 RT\left(n_{salt2}\right)_{high}\left\{\ln\left[\left(m_{salt2}\right)_{high}\left(\gamma_{\pm salt2}\right)_{high}\right] - \phi_{high}\right\} \end{aligned} \tag{33}$$

where ν_1 and ν_2 are stoichiometric coefficients of salt1 and salt2, respectively. Also $\nu_1 = \nu_2 = 2$.

As one can see from Table 5, the $\Delta_{mix}G$ value of each mixture is improved to some extent compared with that of the NaCl system, and the $\Delta_{mix}G$ value is consistent with the variation rule of the $\Delta\phi_{cell\text{-}mix}$ value. In contrast to the NaCl system, the smallest performance improvement is the mixture containing LiAc, with an increase of about 8%–11%; while the performance of the KAc + RbAc, KAc + CsAc and RbAc + CsAc systems have been significantly improved, with an increase of about 17%–18%.

In conclusion, the $\Delta\phi_{cell\text{-}mix}$ and $\Delta_{mix}G$ values of alkali acetate mixtures are higher than those of the NaCl system at the same concentration conditions, and the KAc + RbAc, KAc + CsAc and RbAc + CsAc systems show relatively obvious performance improvements.

5. Comparison of pure alkali acetate salts and their mixtures

Fig. 7 gives the comparison of the ideal cell potential difference of pure alkali acetate salts and their mixtures. The mixture-$\Delta\phi_{cell\text{-}mix}$ is found to be included in the range between the two pure salt-$\Delta\phi_{cell\text{-}pure}$ cases. It is not surprising to get such a result. We know that the difference in activity coefficient value between pure salt and mixture at low concentration (i.e. m = 0.1 mol kg^{-1}) is very small, so the difference between Eqs. (31) and (27) can be approximated as:

$$\Delta\phi_{cell\text{-}mix} - \Delta\phi_{cell\text{-}pure} \approx \frac{RT}{F}\ln\left[\frac{\gamma^{*high}_{\pm salt1\text{-}mix}\gamma^{*high}_{\pm salt2\text{-}mix}}{\left(\gamma^{*high}_{\pm salt\text{-}pure}\right)^2}\right] \tag{34}$$

As discussed in section 4.2, in contrast to pure salt case, the activity coefficient of each salt in the mixture will increase or decrease correspondingly. Taking the LiAc + CsAc system as an example, when $\gamma_{\pm LiAc,pure} < \gamma_{\pm CsAc,pure}$, then $\gamma_{\pm LiAc,mix} > \gamma_{\pm LiAc,pure}$, $\gamma_{\pm CsAc,mix} < \gamma_{\pm CsAc,pure}$ and $\gamma_{\pm LiAc,mix} < \gamma_{\pm CsAc,mix}$. Hence, from Eq. (34), we get $\Delta\phi_{cell\text{-}LiAc} < \Delta\phi_{cell\text{-}mix} < \Delta\phi_{cell\text{-}CsAc}$. For the KAc + CsAc and RbAc + CsAc systems whose activity coefficients do not conform to

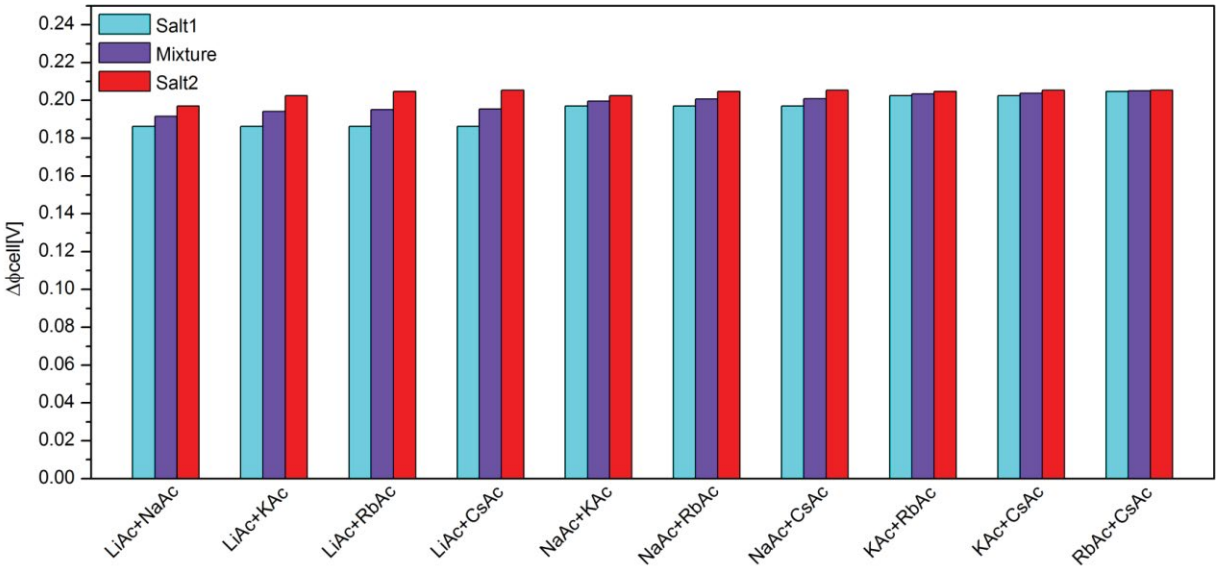

Fig. 7. Comparison of the ideal cell potential difference values between mixtures and the corresponding pure salts.

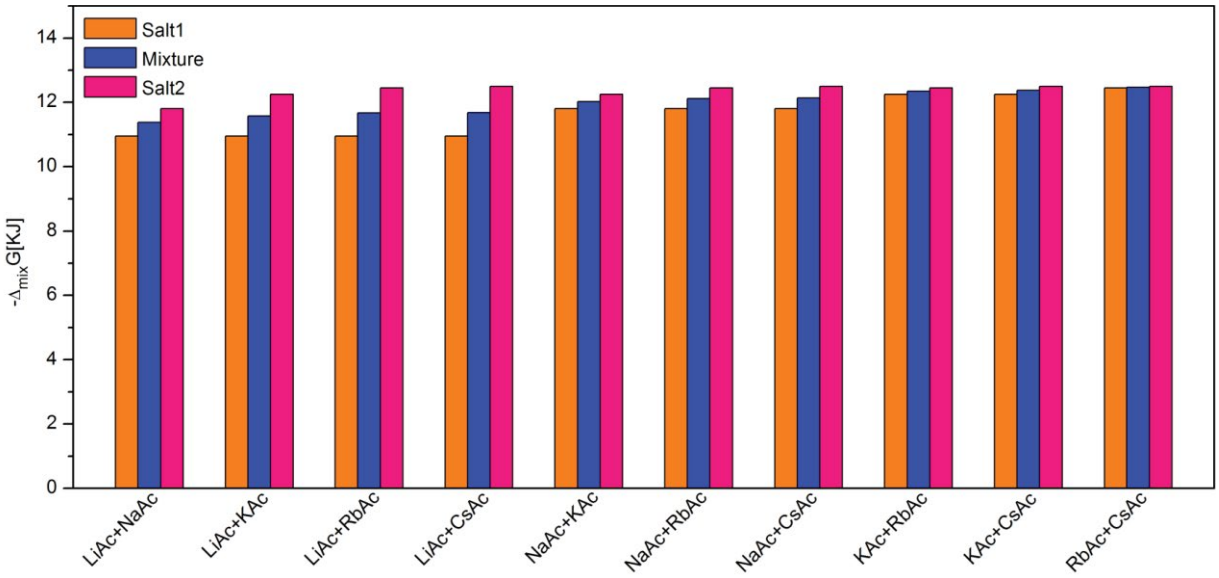

Fig. 8. Comparison of the Gibbs free energy of mixing between mixtures and the corresponding pure salts.

the above rules, but the above results can also be obtained due to the difference in activity coefficient values.

Fig. 8 gives the comparison of the Gibbs free energy of mixing of pure alkali acetate salts and their mixtures. The mixture-$\Delta_{mix}G$ is also found to be included in the range between the two pure salt-$\Delta_{mix}G$ cases and the results are consistent with the variation of the $\Delta\phi_{cell\text{-}mix}$ values.

Figs. 9 and 10 show more directly the improvement effect of various pure salts and various mixtures with respect to the NaCl system. In general, KAc, RbAc and CsAc, as well as their mixtures, have relatively high ideal cell potential difference and Gibbs free energy of mixing.

However, we can also see that the use of mixtures does not add any benefit in terms of thermodynamic modeling point of view, the performance of salt2 is always superior to that of the mixture, and the pure CsAc system provides almost the maximum values of ideal cell potential differences and Gibbs free energy of mixing.

6. Conclusions

The ideal cell potential difference and Gibbs free energy of mixing of alkali acetates and their mixtures were systematically predicted by eMIVM. The results indicated that the activity coefficients of alkali acetates and their mixtures were higher than those of NaCl aqueous solution at the same concentration, so the ideal cell potential difference and Gibbs free energy of mixing of alkali acetates and their mixtures were increased in comparison with the NaCl system. Among those systems, the KAc, RbAc and

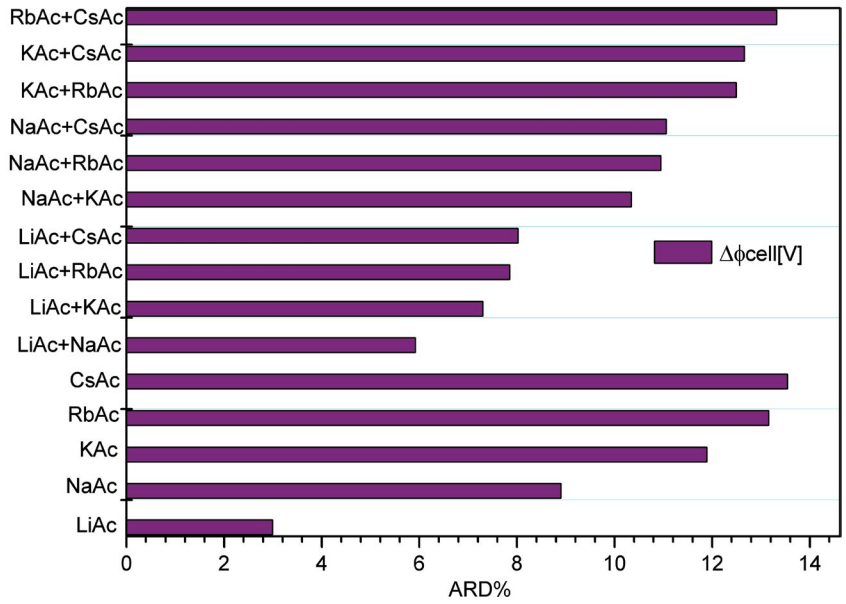

Fig. 9. Comparison of the average relative deviations (ARD%) of the ideal cell potential difference for mixtures and pure salts with respect to the NaCl system.

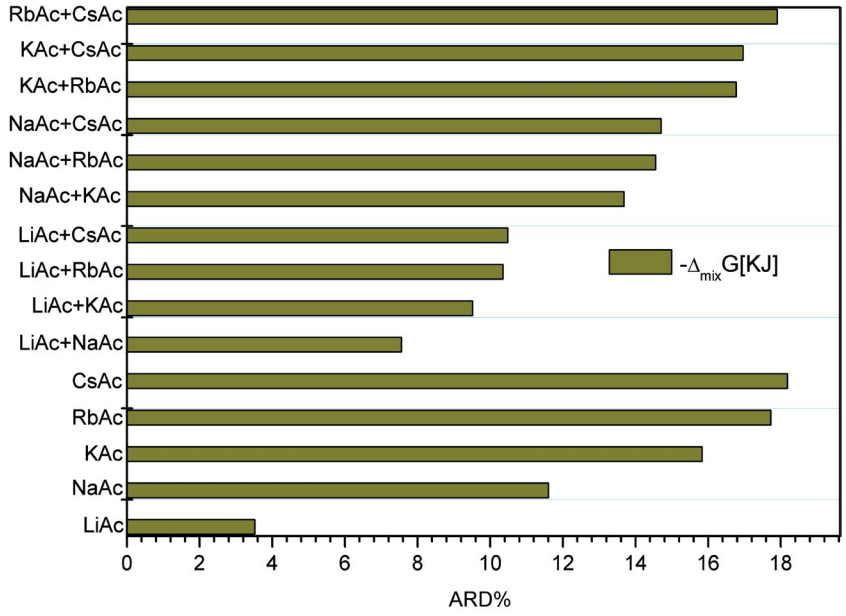

Fig. 10. Comparison of the average relative deviations (ARD%) of the Gibbs free energy of mixing for mixtures and pure salts with respect to the NaCl system.

CsAc systems and their mixtures have relatively high activity coefficients, resulting in relatively high values of ideal cell potential difference and Gibbs free energy of mixing. Nevertheless, from the thermodynamic modeling point of view, there is no benefit from using mixtures. The performance of salt2 is always better than that of the mixture, and the pure CsAc system provides almost the maximum values of ideal cell potential difference and Gibbs free energy of mixing. Moreover, the research of the application of non-conventional salt in the closed-loop RED unit is still in its infancy, and there is still a lot of work to be done in the future.

Acknowledgement

This work was financially supported by the National Natural Science Foundation of China under Grant No. 51464022.

References

[1] Z.J. Jia, B.G. Wang, S.Q. Song, Y.S. Fan, Blue energy: current technologies for sustainable power generation from water salinity gradient, Renewable Sustainable Energy Rev., 31 (2014) 91–100.

[2] R.A. Tufa, S. Pawlowski, J. Veerman, K. Bouzek, E. Fontananova, G. di Profio, S. Velizarov, J.G. Crespo, K. Nijmeijer, E. Curcio, Progress and prospects in reverse electrodialysis for salinity gradient energy conversion and storage, Appl. Energy, 225 (2018) 290–331.

[3] Y. Mei, C.Y. Tang, Recent developments and future perspectives of reverse electrodialysis technology: a review, Desalination, 425 (2018) 156–174.

[4] O. Schaetzle, C.J.N. Buisman, Salinity gradient energy: current state and new trends, Engineering, 1 (2015) 164–166.

[5] B. Ortega-Delgado, F. Giacalone, A. Cipollina, M. Papapetrou, G. Kosmadakis, A. Tamburini, G. Micale, Boosting the performance of a reverse electrodialysis – multi-effect distillation heat engine by novel solutions and operating conditions, Appl. Energy, 253 (2019) 113489.

[6] F. Giacalone, C. Olkis, G. Santori, A. Cipollina, S. Brandani, G. Micale, Novel solutions for closed-loop reverse electrodialysis: thermodynamic characterisation and perspective analysis, Energy, 166 (2019) 674–689.

[7] A. Tamburini, M. Tedesco, A. Cipollina, G. Micale, M. Ciofalo, M. Papapetrou, W. Van Baak, A. Piacentino, Reverse electrodialysis heat engine for sustainable power production, Appl. Energy, 206 (2017) 1334–1353.

[8] J. Veerman, M. Saakes, S.J. Metz, G.J. Harmsen, Reverse electrodialysis: a validated process model for design and optimization, Chem. Eng. J., 166 (2011) 256–268.

[9] R. Ortiz-Imedio, L. Gomez-Coma, M. Fallanza, A. Ortiz, R. Ibañez, I. Ortiz, Comparative performance of salinity gradient power-reverse electrodialysis under different operating conditions, Desalination, 457 (2019) 8–21.

[10] F. Giacalone, P. Catrini, A. Tamburini, A. Cipollina, A. Piacentino, G. Micale, Exergy analysis of reverse electrodialysis, Energy Convers. Manage., 164 (2018) 588–602.

[11] P. Palenzuela, M. Micari, B. Ortega-Delgado, F. Giacalone, G. Zaragoza, D.-C. Alarcón-Padilla, A. Cipollina, A. Tamburini, G. Micale, Performance analysis of a RED-MED salinity gradient heat engine, Energies, 11 (2018) 3385.

[12] J.G. Hong, W. Zhang, J. Luo, Y.S. Chen, Modeling of power generation from the mixing of simulated saline and freshwater with a reverse electrodialysis system: the effect of monovalent and multivalent ions, Appl. Energy, 110 (2013) 244–251.

[13] L. Gómez-Coma, V.M. Ortiz-Martínez, J. Carmona, L. Palacio, P. Prádanos, M. Fallanza, A. Ortiz, R. Ibañez, I. Ortiz, Modeling the influence of divalent ions on membrane resistance and electric power in reverse electrodialysis, J. Membr. Sci., 592 (2019) 117385.

[14] M.C. Hatzell, I. Ivanov, R.D. Cusick, X. Zhu, B.E. Logan, Comparison of hydrogen production and electrical power generation for energy capture in closed-loop ammonium bicarbonate reverse electrodialysis systems, Phys. Chem. Chem. Phys., 16 (2014) 1632–1638.

[15] R.D. Cusick, Y. Kim, B.E. Logan, Energy capture from thermolytic solutions in microbial reverse-electrodialysis cells, Science, 335 (2012) 1474–1477.

[16] F. Giacalone, F. Vassallo, F. Scargiali, A. Tamburini, A. Cipollina, G. Micale, The first operating thermolytic reverse electrodialysis heat engine, J. Membr. Sci., 595 (2020) 117522.

[17] F. Giacalone, F. Vassallo, L. Griffin, M.C. Ferrari, G. Micale, F. Scargiali, A. Tamburini, A. Cipollina, Thermolytic reverse electrodialysis heat engine: model development, integration and performance analysis, Energy Convers. Manage., 189 (2019) 1–13.

[18] X.P. Zhu, W.H. He, B.E. Logan, Influence of solution concentration and salt types on the performance of reverse electrodialysis cells, J. Membr. Sci., 494 (2015) 154–160.

[19] C. Olkis, G. Santori, S. Brandani, An adsorption reverse electrodialysis system for the generation of electricity from low-grade heat, Appl. Energy, 231 (2018) 222–234.

[20] F. Giacalone, A. Tamburini, A. Cipollina, G. Micale, Reverse electrodialysis – multi effect distillation heat engine fed by lithium chloride solutions, Chem. Eng. Trans., 74 (2019) 787–790, doi: 10.3303/CET1974132.

[21] M. Micari, M. Bevacqua, A. Cipollina, A. Tamburini, W. Van Baak, T. Putts, G. Micale, Effect of different aqueous solutions of pure salts and salt mixtures in reverse electrodialysis systems for closed-loop applications, J. Membr. Sci., 551 (2018) 315–325.

[22] C.Y. Zhang, Y.B. Xing, D.P. Tao, Prediction of activity and osmotic coefficients of fission product systems CsOH + CsX (X = Cl, Br, I) at 298.15 K, J. Radioanal. Nucl. Chem., 323 (2020) 773–784.

[23] D.P. Tao, A new model of thermodynamics of liquid mixtures and its application to liquid alloys, Thermochim. Acta, 363 (2000) 105–113.

[24] K.S. Pitzer, Electrolytes. From dilute solutions to fused salts, J. Am. Chem. Soc., 102 (1980) 2902–2906.

[25] Y. Marcus, Ionic volumes in solution, Biophys. Chem., 124 (2006) 200–207.

[26] A. Haghtalab, K. Peyvandi, Electrolyte-UNIQUAC-NRF model for the correlation of the mean activity coefficient of electrolyte solutions, Fluid Phase Equilib., 281 (2009) 163–171.

[27] R.A. Robinson, R.H. Stokes, Electrolyte Solutions, 2nd revised edition, Dover Publications, New York, 2002.

[28] N.Y. Yip, D. Brogioli, H.V.M. Hamelers, K. Nijmeijer, Salinity gradients for sustainable energy: primer, progress, and prospects, Environ. Sci. Technol., 50 (2016) 12072–12094.

[29] J.M. Prausnitz, R.N. Lichtenthaler, E.G. de Azevedo, Molecular Thermodynamics of Fluid-Phase Equilibria, Prentice-Hall, New York, 1998.

[30] R.A. Robinson, R.H. Wood, P.J. Reilly, Calculation of excess Gibbs energies and activity coefficients from isopiestic measurements on mixtures of lithium and sodium salts, J. Chem. Thermodyn., 3 (1971) 461–471.

[31] R.A. Jones, J.E. Prue, Excess Gibbs energies of aqueous mixtures of sodium chloride, potassium chloride, sodium acetate, and potassium acetate at 25°C, J. Solution Chem., 3 (1974) 585–592.

[32] R.D. Lanier, Activity coefficients of sodium chloride in aqueous three-component solutions by cation-sensitive glass electrodes[1a], J. Phys. Chem., 69 (1965) 3992–3998.

[33] S. Manohar, J. Ananthaswamy, Activity coefficients of NaCl in NaCl–NaOAc–H_2O at 25, 35, and 45°C, Can. J. Chem., 69 (1991) 111–115.

[34] F. Hernández-Luis, L. Fernández-Mérida, O. González-Díaz, M.A. Esteso, S.-K. Khoo, T.-K. Lim, Activity coefficients of the systems: NaBr + Na-Acetate + H_2O and NaBr + Na-Propionate + H_2O at 25°C. Application of Scatchard's, Pitzer's and Lim's methods, Ber. Bunsenges. Phys. Chem., 97 (1993) 229–234.

Supporting information

S1. Correlation and prediction of activity and osmotic coefficients of alkali acetates and their mixtures by electrolyte molecular interaction volume model (eMIVM) at 298.15 K

Note: m = 0.1–3.5 mol kg^{-1} for pure salt; I = 0.1–3.5 mol kg^{-1} for mixture, m-salt$A$ = m-salt$B$. Tables S1–S10 give the prediction values of eMIVM.

Table S1
The activity and osmotic coefficients of the LiAc + NaAc system

	LiAc		NaAc			LiAc(A) + NaAc(B)		
m-mol kg^{-1}	OS	AC	OS	AC	I-mol kg^{-1}	OS	AC-A	AC-B
0.1	0.9335	0.7795	0.9382	0.7869	0.1	0.9358	0.7821	0.7842
0.2	0.9263	0.737	0.9356	0.7509	0.2	0.9309	0.7419	0.7459
0.3	0.9258	0.7148	0.9395	0.7348	0.3	0.9326	0.7218	0.7276
0.4	0.9282	0.7016	0.9461	0.7275	0.4	0.937	0.7105	0.7181
0.5	0.9322	0.6934	0.9541	0.7252	0.5	0.943	0.7044	0.7136
0.6	0.9371	0.6886	0.9629	0.7261	0.6	0.9499	0.7014	0.7124
0.7	0.9427	0.6861	0.9723	0.7292	0.7	0.9573	0.7008	0.7135
0.8	0.9487	0.6852	0.9819	0.734	0.8	0.9651	0.7018	0.7162
0.9	0.9551	0.6857	0.9917	0.7401	0.9	0.9732	0.7041	0.7202
1	0.9617	0.6872	1.0017	0.7472	1	0.9814	0.7074	0.7253
1.2	0.9752	0.6925	1.0215	0.7637	1.2	0.9981	0.7163	0.7377
1.4	0.9891	0.7002	1.0412	0.7826	1.4	1.0148	0.7275	0.7525
1.6	1.0029	0.7096	1.0605	0.8033	1.6	1.0314	0.7404	0.7691
1.8	1.0168	0.7203	1.0794	0.8253	1.8	1.0477	0.7545	0.787
2	1.0304	0.732	1.0977	0.8484	2	1.0637	0.7696	0.8059
2.5	1.0633	0.7644	1.1409	0.9095	2.5	1.1017	0.8105	0.8566
3	1.0942	0.7997	1.1802	0.974	3	1.1368	0.8542	0.9106
3.5	1.1227	0.8367	1.2158	1.0405	3.5	1.1688	0.8994	0.9665

OS refers to osmotic coefficient
AC refers to activity coefficient

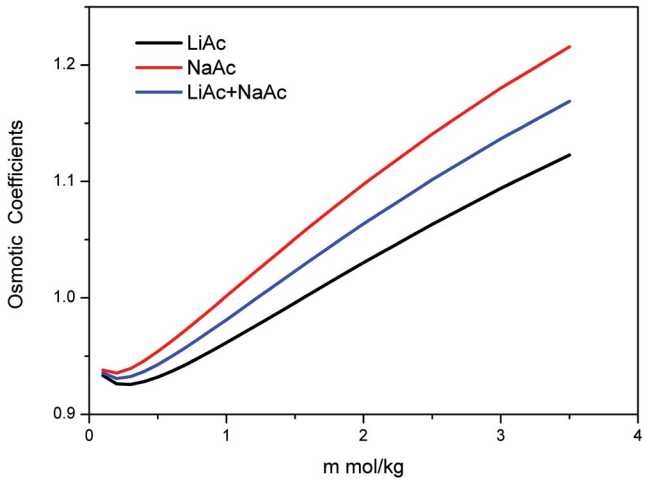

Fig. S1. Osmotic Coefficients of the LiAc, NaAc and LiAc + NaAc systems.

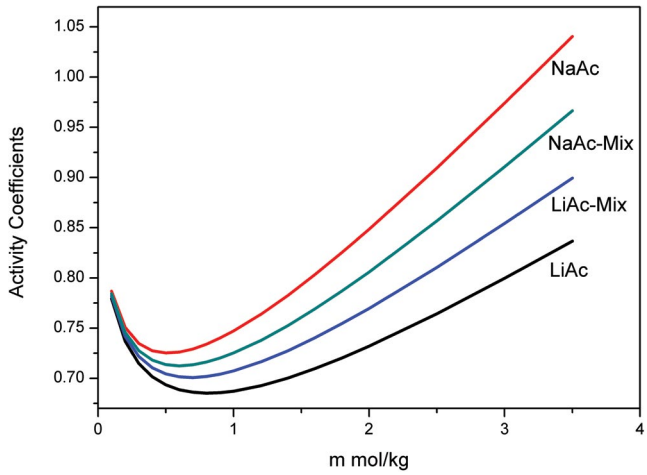

Fig. S2. Activity Coefficients of the LiAc, NaAc and LiAc + NaAc systems, also $\gamma_{\pm NaAc,mix} < \gamma_{\pm NaAc,pure}$ and $\gamma_{\pm LiAc,mix} > \gamma_{\pm LiAc,pure}$.

Table S2
The activity and osmotic coefficients of the LiAc + KAc system

m-mol kg^{-1}	LiAc		KAc		LiAc(*A*) + KAc(*B*)			
	OS	AC	OS	AC	I-mol kg^{-1}	OS	AC-*A*	AC-*B*
0.1	0.9335	0.7795	0.9398	0.7893	0.1	0.9365	0.7824	0.7859
0.2	0.9263	0.737	0.9387	0.7556	0.2	0.9322	0.7425	0.7491
0.3	0.9258	0.7148	0.9441	0.7417	0.3	0.9346	0.7227	0.7323
0.4	0.9282	0.7016	0.9523	0.7366	0.4	0.9397	0.7118	0.7244
0.5	0.9322	0.6934	0.9619	0.7366	0.5	0.9464	0.706	0.7215
0.6	0.9371	0.6886	0.9723	0.7399	0.6	0.954	0.7035	0.7219
0.7	0.9427	0.6861	0.9833	0.7454	0.7	0.9621	0.7032	0.7246
0.8	0.9487	0.6852	0.9945	0.7527	0.8	0.9707	0.7047	0.729
0.9	0.9551	0.6857	1.006	0.7614	0.9	0.9795	0.7074	0.7348
1	0.9617	0.6872	1.0175	0.7712	1	0.9885	0.7112	0.7416
1.2	0.9752	0.6925	1.0406	0.7934	1.2	1.0067	0.7211	0.7578
1.4	0.9891	0.7002	1.0635	0.8182	1.4	1.025	0.7334	0.7766
1.6	1.0029	0.7096	1.086	0.8452	1.6	1.0431	0.7474	0.7972
1.8	1.0168	0.7203	1.1079	0.8739	1.8	1.0609	0.7628	0.8195
2	1.0304	0.732	1.1293	0.9039	2	1.0783	0.7792	0.843
2.5	1.0633	0.7644	1.1798	0.984	2.5	1.12	0.8235	0.9059
3	1.0942	0.7997	1.226	1.0692	3	1.1585	0.8709	0.9732
3.5	1.1227	0.8367	1.2679	1.1582	3.5	1.1938	0.9201	1.0436

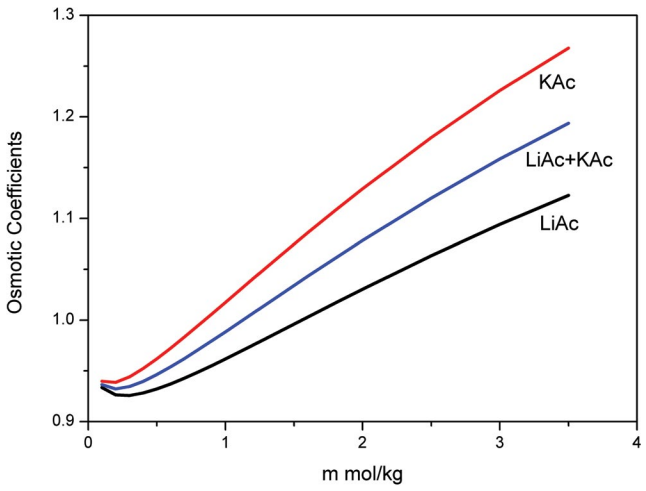

Fig. S3. Osmotic Coefficients of the LiAc, KAc and LiAc + KAc systems.

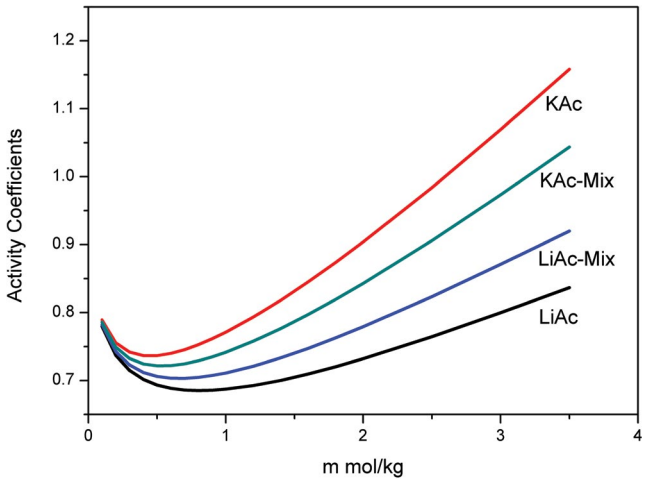

Fig. S4. Activity Coefficients of the LiAc, KAc and LiAc + KAc systems, also $\gamma_{\pm KAc,mix} < \gamma_{\pm KAc,pure}$ and $\gamma_{\pm LiAc,mix} > \gamma_{\pm LiAc,pure}$.

Table S3
The activity and osmotic coefficients of the LiAc + RbAc system

m-mol kg^{-1}	LiAc		RbAc		LiAc(*A*) + RbAc(*B*)			
	OS	AC	OS	AC	I-mol kg^{-1}	OS	AC-*A*	AC-*B*
0.1	0.9335	0.7795	0.9402	0.79	0.1	0.9366	0.7823	0.7863
0.2	0.9263	0.737	0.9395	0.7568	0.2	0.9324	0.7423	0.7498
0.3	0.9258	0.7148	0.9455	0.7436	0.3	0.9349	0.7224	0.7334
0.4	0.9282	0.7016	0.9542	0.7393	0.4	0.9402	0.7115	0.726
0.5	0.9322	0.6934	0.9644	0.74	0.5	0.9471	0.7057	0.7236
0.6	0.9371	0.6886	0.9754	0.7441	0.6	0.9549	0.7032	0.7245
0.7	0.9427	0.6861	0.987	0.7506	0.7	0.9633	0.703	0.7277
0.8	0.9487	0.6852	0.9989	0.7589	0.8	0.9722	0.7045	0.7327
0.9	0.9551	0.6857	1.011	0.7686	0.9	0.9813	0.7074	0.7391
1	0.9617	0.6872	1.0233	0.7794	1	0.9905	0.7113	0.7466
1.2	0.9752	0.6925	1.0478	0.804	1.2	1.0094	0.7215	0.7642
1.4	0.9891	0.7002	1.0722	0.8314	1.4	1.0283	0.7341	0.7845
1.6	1.0029	0.7096	1.0962	0.8612	1.6	1.0471	0.7485	0.8069
1.8	1.0168	0.7203	1.1197	0.893	1.8	1.0657	0.7644	0.831
2	1.0304	0.732	1.1426	0.9264	2	1.0839	0.7813	0.8565
2.5	1.0633	0.7644	1.197	1.0158	2.5	1.1274	0.8272	0.9251
3	1.0942	0.7997	1.247	1.1119	3	1.1679	0.8764	0.9989
3.5	1.1227	0.8367	1.2926	1.2131	3.5	1.205	0.9277	1.0765

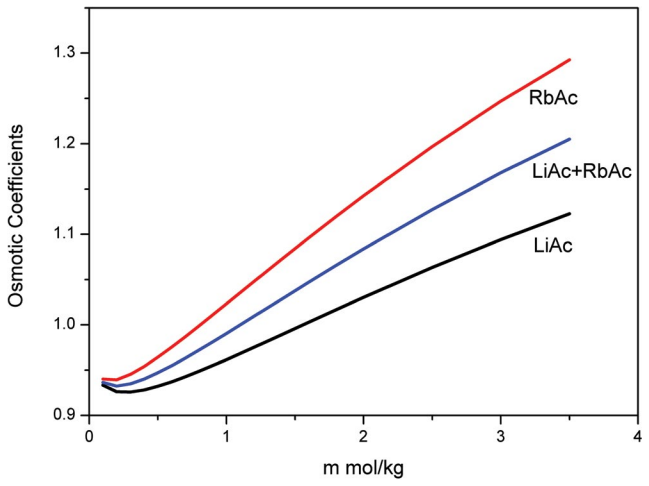

Fig. S5. Osmotic Coefficients of the LiAc, RbAc and LiAc + RbAc systems.

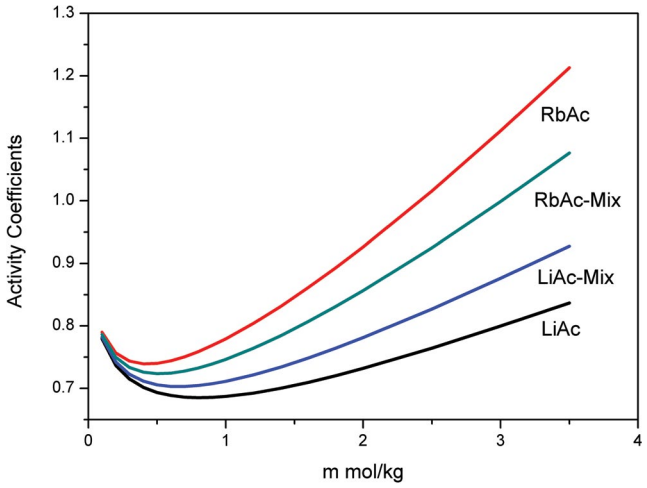

Fig. S6. Activity Coefficients of the LiAc, KAc and LiAc + KAc systems, also $\gamma_{\pm RbAc,mix} < \gamma_{\pm RbAc,pure}$ and $\gamma_{\pm LiAc,mix} > \gamma_{\pm LiAc,pure}$.

Table S4
The activity and osmotic coefficients of the LiAc + CsAc system

	LiAc		CsAc		LiAc(*A*) + CsAc(*B*)			
m-mol kg^{-1}	OS	AC	OS	AC	I-mol kg^{-1}	OS	AC-*A*	AC-*B*
0.1	0.9335	0.7795	0.9408	0.7911	0.1	0.9368	0.7821	0.7874
0.2	0.9263	0.737	0.9408	0.7588	0.2	0.933	0.7419	0.7519
0.3	0.9258	0.7148	0.9473	0.7464	0.3	0.9357	0.7218	0.7364
0.4	0.9282	0.7016	0.9565	0.7429	0.4	0.9412	0.7107	0.7298
0.5	0.9322	0.6934	0.9671	0.7444	0.5	0.9482	0.7047	0.7283
0.6	0.9371	0.6886	0.9785	0.7492	0.6	0.9562	0.7019	0.73
0.7	0.9427	0.6861	0.9905	0.7564	0.7	0.9648	0.7014	0.7341
0.8	0.9487	0.6852	1.0027	0.7653	0.8	0.9737	0.7026	0.7399
0.9	0.9551	0.6857	1.0151	0.7756	0.9	0.9829	0.7052	0.7471
1	0.9617	0.6872	1.0275	0.7871	1	0.9922	0.7087	0.7553
1.2	0.9752	0.6925	1.0524	0.8128	1.2	1.0112	0.7183	0.7745
1.4	0.9891	0.7002	1.077	0.8413	1.4	1.0302	0.7302	0.7964
1.6	1.0029	0.7096	1.1011	0.8722	1.6	1.049	0.7438	0.8203
1.8	1.0168	0.7203	1.1247	0.9049	1.8	1.0675	0.7588	0.846
2	1.0304	0.732	1.1476	0.9392	2	1.0857	0.7749	0.873
2.5	1.0633	0.7644	1.2016	1.0306	2.5	1.129	0.8184	0.9455
3	1.0942	0.7997	1.2511	1.1284	3	1.1691	0.865	1.0232
3.5	1.1227	0.8367	1.2959	1.2309	3.5	1.2059	0.9135	1.1048

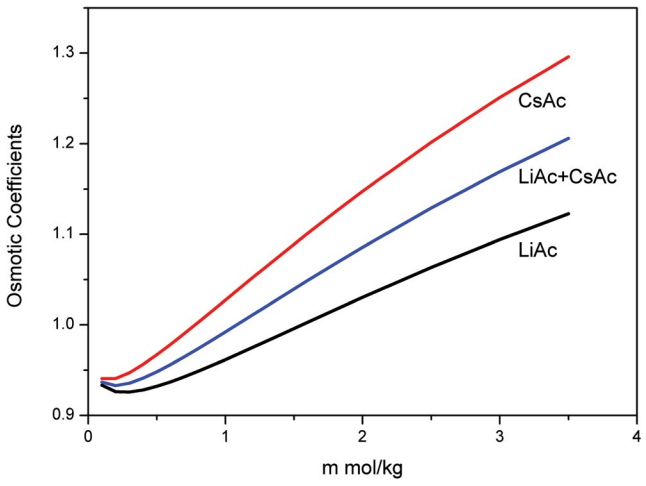

Fig. S7. Osmotic Coefficients of the LiAc, CsAc and LiAc + CsAc systems.

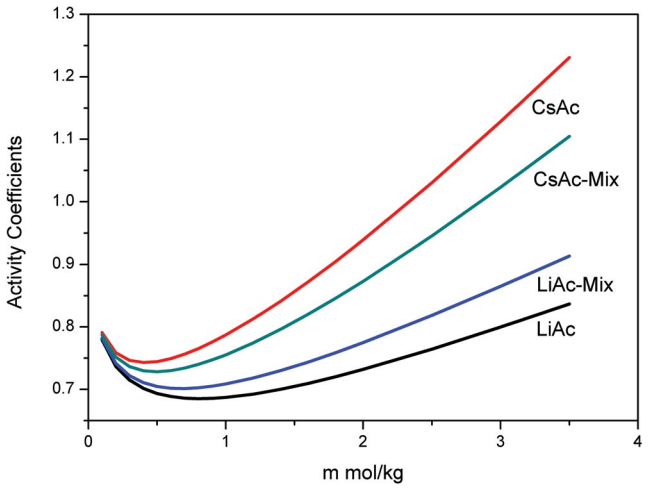

Fig. S8. Activity Coefficients of the LiAc, CsAc and LiAc + CsAc systems, also $\gamma_{\pm CsAc,mix} < \gamma_{\pm CsAc,pure}$ and $\gamma_{\pm LiAc,mix} > \gamma_{\pm LiAc,pure}$.

Table S5
The activity and osmotic coefficients of the NaAc + KAc system

	NaAc		KAc			NaAc(*A*) + KAc(*B*)		
m-mol kg^{-1}	OS	AC	OS	AC	I-mol kg^{-1}	OS	AC-*A*	AC-*B*
0.1	0.9382	0.7869	0.9398	0.7893	0.1	0.9389	0.7874	0.7887
0.2	0.9356	0.7509	0.9387	0.7556	0.2	0.937	0.7518	0.7544
0.3	0.9395	0.7348	0.9441	0.7417	0.3	0.9416	0.7361	0.7399
0.4	0.9461	0.7275	0.9523	0.7366	0.4	0.949	0.7292	0.7343
0.5	0.9541	0.7252	0.9619	0.7366	0.5	0.9577	0.7274	0.7337
0.6	0.9629	0.7261	0.9723	0.7399	0.6	0.9673	0.7287	0.7363
0.7	0.9723	0.7292	0.9833	0.7454	0.7	0.9774	0.7324	0.7412
0.8	0.9819	0.734	0.9945	0.7527	0.8	0.9878	0.7377	0.7479
0.9	0.9917	0.7401	1.006	0.7614	0.9	0.9984	0.7443	0.7558
1	1.0017	0.7472	1.0175	0.7712	1	1.0091	0.752	0.7649
1.2	1.0215	0.7637	1.0406	0.7934	1.2	1.0306	0.7698	0.7855
1.4	1.0412	0.7826	1.0635	0.8182	1.4	1.0518	0.79	0.8088
1.6	1.0605	0.8033	1.086	0.8452	1.6	1.0727	0.8121	0.834
1.8	1.0794	0.8253	1.1079	0.8739	1.8	1.093	0.8356	0.8608
2	1.0977	0.8484	1.1293	0.9039	2	1.1128	0.8603	0.889
2.5	1.1409	0.9095	1.1798	0.984	2.5	1.1596	0.9258	0.9638
3	1.1802	0.974	1.226	1.0692	3	1.2024	0.995	1.0433
3.5	1.2158	1.0405	1.2679	1.1582	3.5	1.2412	1.0667	1.126

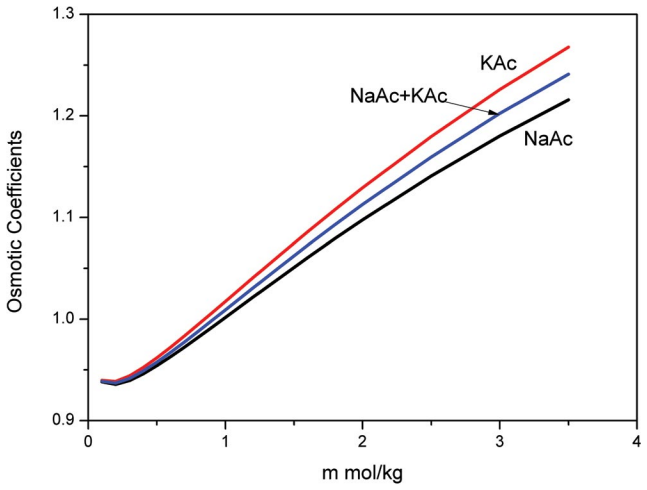

Fig. S9. Osmotic Coefficients of the NaAc, KAc and NaAc + KAc systems.

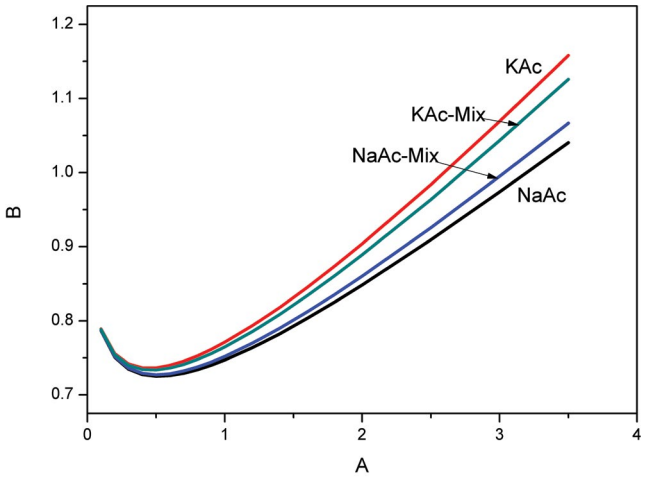

Fig. S10. Activity Coefficients of the NaAc, KAc and NaAc + KAc systems, also $\gamma_{\pm KAc,mix} < \gamma_{\pm KAc,pure}$ and $\gamma_{\pm NaAc,mix} > \gamma_{\pm NaAc,pure}$.

Table S6
The activity and osmotic coefficients of the NaAc + RbAc system

	NaAc		RbAc		NaAc(*A*) + RbAc(*B*)			
m-mol kg^{-1}	OS	AC	OS	AC	I-mol kg^{-1}	OS	AC-*A*	AC-*B*
0.1	0.9382	0.7869	0.9402	0.79	0.1	0.9391	0.7873	0.7892
0.2	0.9356	0.7509	0.9395	0.7568	0.2	0.9373	0.7517	0.7553
0.3	0.9395	0.7348	0.9455	0.7436	0.3	0.9421	0.736	0.7413
0.4	0.9461	0.7275	0.9542	0.7393	0.4	0.9496	0.7292	0.7361
0.5	0.9541	0.7252	0.9644	0.74	0.5	0.9586	0.7274	0.7361
0.6	0.9629	0.7261	0.9754	0.7441	0.6	0.9685	0.7288	0.7393
0.7	0.9723	0.7292	0.987	0.7506	0.7	0.9788	0.7325	0.7448
0.8	0.9819	0.734	0.9989	0.7589	0.8	0.9895	0.738	0.7521
0.9	0.9917	0.7401	1.011	0.7686	0.9	1.0004	0.7448	0.7608
1	1.0017	0.7472	1.0233	0.7794	1	1.0115	0.7526	0.7706
1.2	1.0215	0.7637	1.0478	0.804	1.2	1.0336	0.7708	0.7928
1.4	1.0412	0.7826	1.0722	0.8314	1.4	1.0555	0.7915	0.8178
1.6	1.0605	0.8033	1.0962	0.8612	1.6	1.0771	0.8141	0.8449
1.8	1.0794	0.8253	1.1197	0.893	1.8	1.0982	0.8382	0.8738
2	1.0977	0.8484	1.1426	0.9264	2	1.1188	0.8636	0.9042
2.5	1.1409	0.9095	1.197	1.0158	2.5	1.1675	0.931	0.9853
3	1.1802	0.974	1.247	1.1119	3	1.2122	1.0026	1.0721
3.5	1.2158	1.0405	1.2926	1.2131	3.5	1.2528	1.0768	1.163

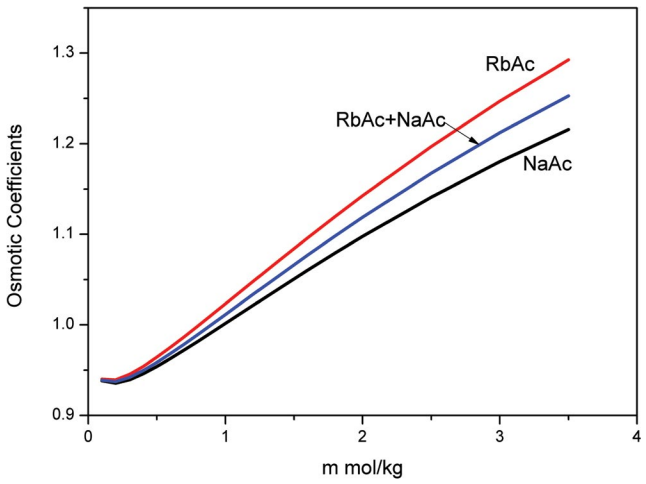

Fig. S11. Osmotic Coefficients of the NaAc, RbAc and NaAc + RbAc systems.

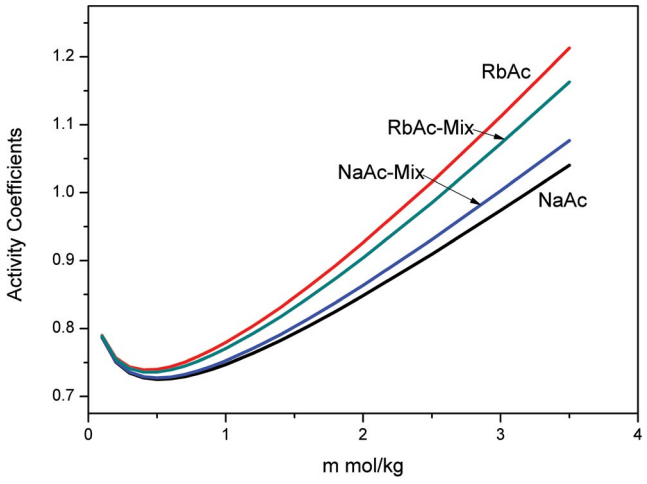

Fig. S12. Activity Coefficients of the NaAc, KAc and NaAc + KAc systems, also $\gamma_{\pm RbAc,mix} < \gamma_{\pm RbAc,pure}$ and $\gamma_{\pm NaAc,mix} > \gamma_{\pm NaAc,pure}$.

Table S7
The activity and osmotic coefficients of the NaAc + CsAc system

	NaAc		CsAc			NaAc(*A*) + CsAc(*B*)		
m-mol kg^{-1}	OS	AC	OS	AC	I-mol kg^{-1}	OS	AC-*A*	AC-*B*
0.1	0.9382	0.7869	0.9408	0.7911	0.1	0.9393	0.7871	0.7903
0.2	0.9356	0.7509	0.9408	0.7588	0.2	0.9378	0.7512	0.7574
0.3	0.9395	0.7348	0.9473	0.7464	0.3	0.9428	0.7353	0.7443
0.4	0.9461	0.7275	0.9565	0.7429	0.4	0.9506	0.7282	0.7401
0.5	0.9541	0.7252	0.9671	0.7444	0.5	0.9597	0.7262	0.7409
0.6	0.9629	0.7261	0.9785	0.7492	0.6	0.9697	0.7273	0.7449
0.7	0.9723	0.7292	0.9905	0.7564	0.7	0.9802	0.7308	0.7513
0.8	0.9819	0.734	1.0027	0.7653	0.8	0.9911	0.7359	0.7594
0.9	0.9917	0.7401	1.0151	0.7756	0.9	1.0021	0.7423	0.769
1	1.0017	0.7472	1.0275	0.7871	1	1.0132	0.7498	0.7796
1.2	1.0215	0.7637	1.0524	0.8128	1.2	1.0354	0.7672	0.8035
1.4	1.0412	0.7826	1.077	0.8413	1.4	1.0574	0.7871	0.8302
1.6	1.0605	0.8033	1.1011	0.8722	1.6	1.079	0.8088	0.859
1.8	1.0794	0.8253	1.1247	0.9049	1.8	1.1001	0.832	0.8896
2	1.0977	0.8484	1.1476	0.9392	2	1.1206	0.8563	0.9217
2.5	1.1409	0.9095	1.2016	1.0306	2.5	1.1691	0.921	1.0072
3	1.1802	0.974	1.2511	1.1284	3	1.2135	0.9894	1.0984
3.5	1.2158	1.0405	1.2959	1.2309	3.5	1.2537	1.0601	1.1938

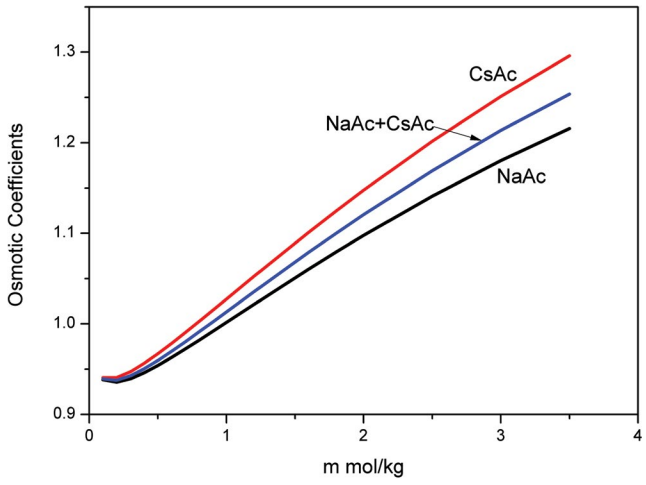

Fig. S13. Osmotic Coefficients of the NaAc, CsAc and NaAc + CsAc systems.

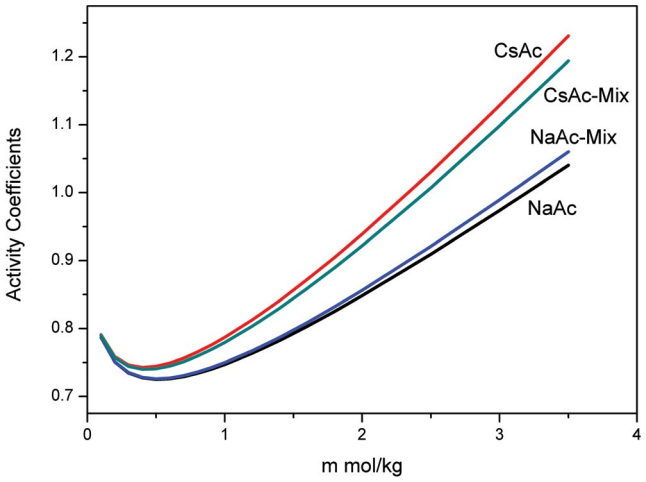

Fig. S14. Activity Coefficients of the NaAc, CsAc and NaAc + CsAc systems, also $\gamma_{\pm CsAc,mix} < \gamma_{\pm CsAc,pure}$ and $\gamma_{\pm NaAc,mix} > \gamma_{\pm NaAc,pure}$.

Table S8
The activity and osmotic coefficients of the KAc + RbAc system

	KAc		RbAc		KAc(*A*) + RbAc(*B*)			
m-mol kg^{-1}	OS	AC	OS	AC	I-mol kg^{-1}	OS	AC-*A*	AC-*B*
0.1	0.9398	0.7893	0.9402	0.79	0.1	0.9399	0.7894	0.7899
0.2	0.9387	0.7556	0.9395	0.7568	0.2	0.9391	0.7556	0.7566
0.3	0.9441	0.7417	0.9455	0.7436	0.3	0.9447	0.7419	0.7433
0.4	0.9523	0.7366	0.9542	0.7393	0.4	0.9532	0.7369	0.7388
0.5	0.9619	0.7366	0.9644	0.74	0.5	0.963	0.737	0.7394
0.6	0.9723	0.7399	0.9754	0.7441	0.6	0.9738	0.7404	0.7433
0.7	0.9833	0.7454	0.987	0.7506	0.7	0.985	0.7461	0.7496
0.8	0.9945	0.7527	0.9989	0.7589	0.8	0.9966	0.7537	0.7576
0.9	1.006	0.7614	1.011	0.7686	0.9	1.0084	0.7625	0.7671
1	1.0175	0.7712	1.0233	0.7794	1	1.0203	0.7725	0.7776
1.2	1.0406	0.7934	1.0478	0.804	1.2	1.0441	0.7952	0.8015
1.4	1.0635	0.8182	1.0722	0.8314	1.4	1.0677	0.8207	0.8283
1.6	1.086	0.8452	1.0962	0.8612	1.6	1.0909	0.8484	0.8574
1.8	1.1079	0.8739	1.1197	0.893	1.8	1.1137	0.8778	0.8883
2	1.1293	0.9039	1.1426	0.9264	2	1.1358	0.9087	0.9207
2.5	1.1798	0.984	1.197	1.0158	2.5	1.1882	0.9911	1.0075
3	1.226	1.0692	1.247	1.1119	3	1.2363	1.0792	1.1006
3.5	1.2679	1.1582	1.2926	1.2131	3.5	1.2801	1.1714	1.1983

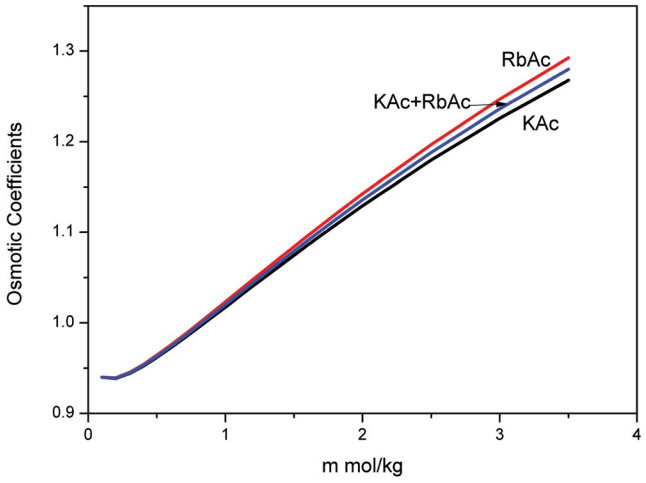

Fig. S15. Osmotic Coefficients of the KAc, RbAc and KAc + RbAc systems.

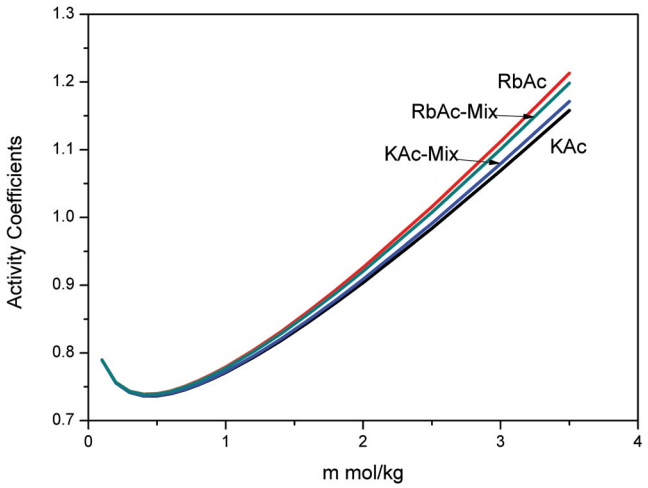

Fig. S16. Activity Coefficients of the KAc, RbAc and KAc + RbAc systems, also $\gamma_{\pm RbAc,mix} < \gamma_{\pm RbAc,pure}$ and $\gamma_{\pm KAc,mix} > \gamma_{\pm KAc,pure}$.

Table S9
The activity and osmotic coefficients of the KAc + CsAc system

	KAc		CsAc		KAc(*A*) + CsAc(*B*)			
m-mol kg^{-1}	OS	AC	OS	AC	I-mol kg^{-1}	OS	AC-A	AC-B
0.1	0.9398	0.7893	0.9408	0.7911	0.1	0.9402	0.7892	0.791
0.2	0.9387	0.7556	0.9408	0.7588	0.2	0.9396	0.7552	0.7588
0.3	0.9441	0.7417	0.9473	0.7464	0.3	0.9456	0.7412	0.7464
0.4	0.9523	0.7366	0.9565	0.7429	0.4	0.9542	0.736	0.7429
0.5	0.9619	0.7366	0.9671	0.7444	0.5	0.9642	0.7359	0.7444
0.6	0.9723	0.7399	0.9785	0.7492	0.6	0.9751	0.739	0.7492
0.7	0.9833	0.7454	0.9905	0.7564	0.7	0.9865	0.7444	0.7563
0.8	0.9945	0.7527	1.0027	0.7653	0.8	0.9983	0.7516	0.7653
0.9	1.006	0.7614	1.0151	0.7756	0.9	1.0101	0.7602	0.7756
1	1.0175	0.7712	1.0275	0.7871	1	1.0221	0.7698	0.7871
1.2	1.0406	0.7934	1.0524	0.8128	1.2	1.046	0.7918	0.8127
1.4	1.0635	0.8182	1.077	0.8413	1.4	1.0698	0.8164	0.8413
1.6	1.086	0.8452	1.1011	0.8722	1.6	1.093	0.8431	0.8721
1.8	1.1079	0.8739	1.1247	0.9049	1.8	1.1158	0.8715	0.9049
2	1.1293	0.9039	1.1476	0.9392	2	1.1379	0.9014	0.9392
2.5	1.1798	0.984	1.2016	1.0306	2.5	1.1901	0.9808	1.0307
3	1.226	1.0692	1.2511	1.1284	3	1.2379	1.0655	1.1286
3.5	1.2679	1.1582	1.2959	1.2309	3.5	1.2813	1.1538	1.2313

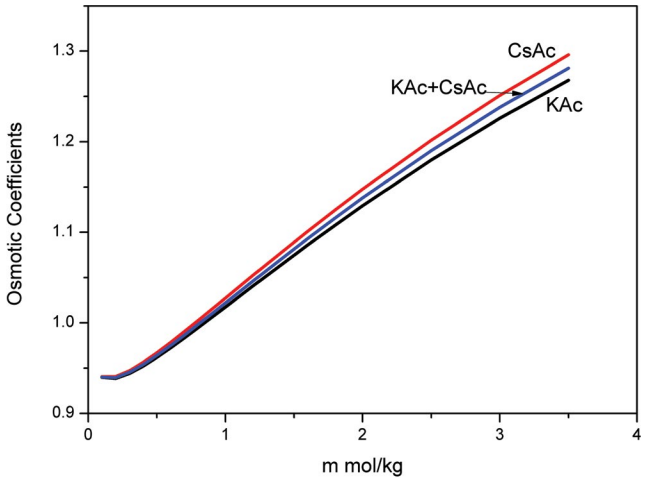

Fig. S17. Osmotic Coefficients of the KAc, CsAc and KAc + CsAc systems.

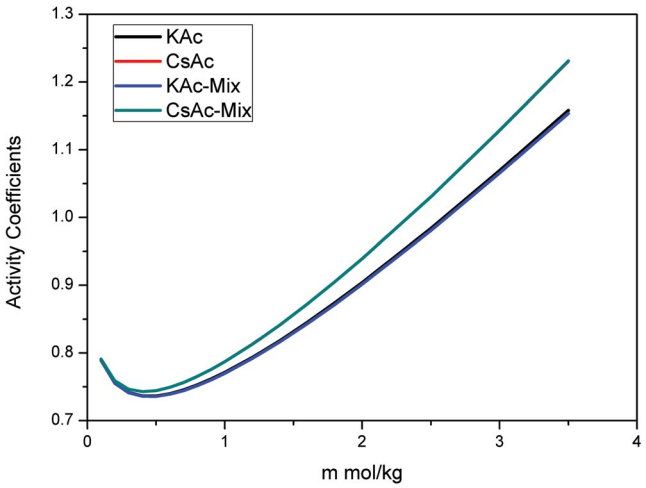

Fig. S18. Activity Coefficients of the KAc, CsAc and KAc + CsAc systems, also $\gamma_{\pm CsAc,mix} > \gamma_{\pm CsAc,pure}$ and $\gamma_{\pm KAc,mix} < \gamma_{\pm KAc,pure}$. But the difference is not obvious.

Table S10
The activity and osmotic coefficients of the RbAc + CsAc system

	RbAc		CsAc		RbAc(*A*) + CsAc(*B*)			
m-mol kg^{-1}	OS	AC	OS	AC	I-mol kg^{-1}	OS	AC-*A*	AC-*B*
0.1	0.9402	0.79	0.9408	0.7911	0.1	0.9405	0.7898	0.7911
0.2	0.9395	0.7568	0.9408	0.7588	0.2	0.9401	0.7564	0.759
0.3	0.9455	0.7436	0.9473	0.7464	0.3	0.9463	0.7429	0.7468
0.4	0.9542	0.7393	0.9565	0.7429	0.4	0.9552	0.7384	0.7434
0.5	0.9644	0.74	0.9671	0.7444	0.5	0.9655	0.7389	0.745
0.6	0.9754	0.7441	0.9785	0.7492	0.6	0.9768	0.7427	0.75
0.7	0.987	0.7506	0.9905	0.7564	0.7	0.9885	0.7488	0.7574
0.8	0.9989	0.7589	1.0027	0.7653	0.8	1.0005	0.7568	0.7666
0.9	1.011	0.7686	1.0151	0.7756	0.9	1.0128	0.7661	0.7772
1	1.0233	0.7794	1.0275	0.7871	1	1.0251	0.7766	0.7889
1.2	1.0478	0.804	1.0524	0.8128	1.2	1.0498	0.8004	0.8152
1.4	1.0722	0.8314	1.077	0.8413	1.4	1.0743	0.827	0.8445
1.6	1.0962	0.8612	1.1011	0.8722	1.6	1.0983	0.8558	0.8762
1.8	1.1197	0.893	1.1247	0.9049	1.8	1.1218	0.8865	0.9098
2	1.1426	0.9264	1.1476	0.9392	2	1.1447	0.9188	0.9451
2.5	1.197	1.0158	1.2016	1.0306	2.5	1.1989	1.0051	1.0393
3	1.247	1.1119	1.2511	1.1284	3	1.2487	1.0977	1.1404
3.5	1.2926	1.2131	1.2959	1.2309	3.5	1.2939	1.1948	1.2468

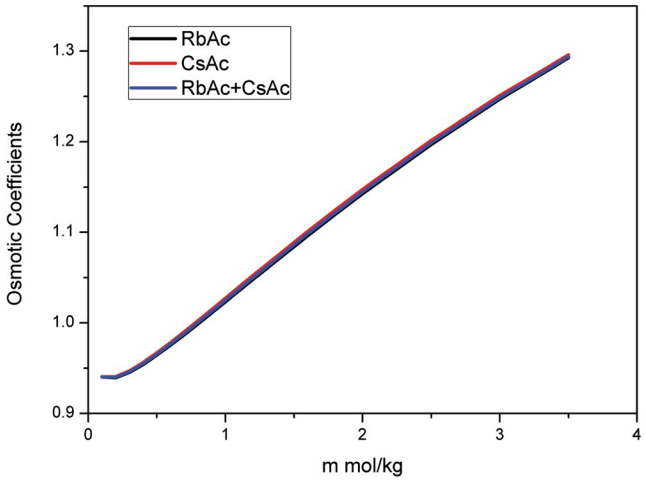

Fig. S19. Osmotic Coefficients of the RbAc, CsAc and RbAc + CsAc systems.

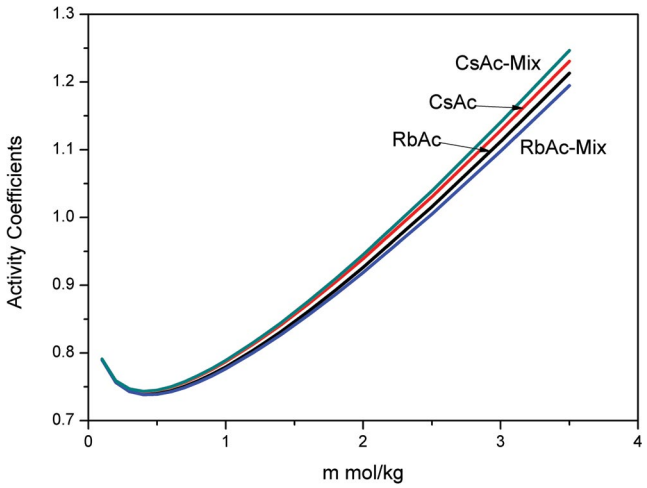

Fig. S20. Activity Coefficients of the RbAc, CsAc and RbAc + CsAc systems, also $\gamma_{\pm CsAc,mix} > \gamma_{\pm CsAc,pure}$ and $\gamma_{\pm RbAc,mix} < \gamma_{\pm RbAc,pure}$.

S2. Prediction results of eMIVM for the mixed systems containing K, Rb, and Cs at 298.15 K

Table S11
Prediction of ternary systems containing K, Rb, and Cs using the eMIVM at 298.15 K

Mixtures	SD-eMIVM	ARD%-eMIVM	Data
NaCl + CsCl	0.0269	2.14	OS
	0.0320	2.72	OS
KCl + CsCl	0.0026	0.22	OS
	0.0014	0.12	OS
KCl + RbCl	0.0104	0.66	OS
RbF + RbCl	0.0065	0.65	AC
CsF + CsCl	0.0074	0.67	AC
CsF + CsBr	0.0073	0.63	AC
RbCl + Rb_2SO_4	0.0297	2.32	AC
CsCl + $BaCl_2$	0.0102	1.08	OS
Overall (10)	0.0134	1.12	

Note: Results in Table S11 are the results of our previous study, which have been submitted to another journal. As shown in the table, eMIVM's prediction results for ternary systems containing K, Rb, and Cs are in good agreement with the experimental data, and the mean standard deviation and average relative deviations (ARD%) are 0.0134 and 1.12%, respectively.